TECHNISCHE
UNIVERSITÄT
WIEN
Vienna University of Technology

DIPLOMARBEIT

Monolithic All-Normal Dispersion Femtosecond Fiber Laser with dynamic adjustable Polarization Control

ausgeführt zum Zwecke der Erlangung des akademischen Grades Diplom-Ingenieur

unter der Leitung von

Univ. Prof. Andrius Baltuška

und

Dr. Alma del Carmen Ferńandez González

Dr. Aart Jan Verhoef

als betreuende Assistentin und betreuender Assistent

am Institut für Photonik E387, Gußhausstrasse 25-29, A-1040 Wien

Eingereicht an der Technischen Universität Wien,

Fakultät für Elektrotechnik und Informationstechnik

von

Tobias Flöry

Wien, November 2011

Abstract

Fiber lasers technology offers unique advantages over conventional bulk laser technology. For example all-normal dispersion fiber cavities can be build more compact, thus more environmental stable and cheaper, and are therefore very attractive for industrial products. The goal of this work is to build and operate a monolithic integrated all-normal dispersion femtosecond fiber oscillator using an all-fiber remote electronically adjustable polarization controller. For this purpose a suitable polarization controller was selected and incorporated into a fiber laser cavity. The fiber laser cavity was designed to operate at all-normal dispersion and therefore does not need any kind of dispersion control or dispersion compensation inside the cavity. In such a configuration the output pulses are highly chirped pulses with picoseconds duration that can be dechirped externally down to the femtosecond regime. For many applications the output energy of modelocked fiber lasers is too low and needs to be amplified. To keep nonlinearities low, thereby preserving pulse quality, the concept of chirped pules amplification is very attractive.

Contents

1. Introduction

The development and application of ultrafast laser sources are of major scientific interest and already have become an important market for industrial needs. Therefore a large number of different technologies were developed and keep developing to satisfy the researchers and industrial needs.

Fiber lasers offer major practical advantages that are [1]:

- With the light confined in a fiber, a laser will not be susceptible to misalignment. The wave-guiding properties of fiber ensure good spatial mode quality.
- Thermal effects are reduced because fibers have a large ratio of surface to volume.
- Fiber laser systems are scalable to high average powers - kilowatt devices exist.
- Fiber components are used in telecommunications industry, so manufacturing costs benefit from economies of scale.

The first fiber laser was proposed and demonstrated in 1961 by E. Snitzer [2, 3] using a neodymium doped glass rod of $30\mu m$ diameter operating around 1.06 μm wavelength.

In 1986 the introduction of low-loss optical fibers doped with rare earth ions [4] lead to the development of new fiber laser systems and revolutionized telecommunications with the availability of erbium doped fiber amplifiers (EDFA) operating at $1.55\mu m$ near the absorption minimum of silica fibers. The introduction of EDFA allowed long-haul communication lines to be established, like transatlantic connections, by having access to compact, robust and more stable fiber laser systems. That attributes are still linked to fiber lasers and amplifiers and fueled the development of new systems.

In 1988 Hanna et al. demonstrated the first ytterbium fiber laser [5], using a 4 μm core pumped at 840 nm, operating from 1035nm to 1084nm. Up to now ytterbium doped fiber lasers have attracted most attention as ytterbium offers some unique advantages over other rare earth elements: the large bandwidth ranging from below 1030nm to above 1100nm, high doping concentration and no excited state absorption.

In 1983 the first modelocked fiber laser was demonstrated [6] and since then nearly all modelocking techniques known from bulk lasers were utilized in fiber technology.

For femtosecond modelocked fiber sources, as well as for every femtosecond laser source, it is crucial to compensate for dispersion and nonlinearities. The most common way to control / compensate group velocity dispersion, which is a main source of pulse broadening, relies on prisms pairs [7], diffraction gratings [8] or chirped mirrors [9]. Those are bulky components and hard to integrate in a monolithic fiber laser.

One recent development is the all-normal-dispersion (ANDi) fiber laser that was first demonstrated by Chong at al. in 2006 that relies on strong pulse-shaping based on spectral filtering of a highly-chirped pulse in the cavity [10]. This scheme produces highly chirped picosecond pulses, which are dechirped to 170 fs outside the laser cavity with pulse energies of up to 3nJ. Through investigation and by optimizing the all-normal dispersion cavity pulse, energies up to 20nJ were reported one year later [11].

The use of all-normal dispersion components in a fiber laser allows to integrate the laser in a monolithic way without the need for any intercavity dispersion compensation. Thus ANDi type lasers, which show quite high output energies compared to soliton lasers, seem to be an adequate choice for reliable femtosecond sources.

2. Fibers

2.1. Basic Fiber Parameters

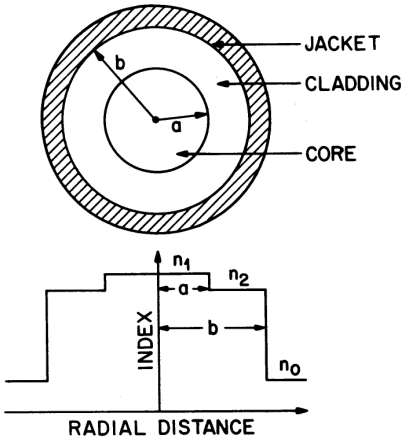

Figure 1: Refractive index profile of a simple step-index fiber [12]

The propagation of light in an optical fiber is based on total internal reflection between a core with refractive index n_1 and a cladding layer which refractive index n_2 where the cladding index n_2 is slightly lower than the core index n_1 as shown in Figure 1. That difference is an important fiber parameter and expressed by the relative index difference Δ:

$$\Delta = \frac{{n_1}^2 - {n_2}^2}{2{n_1}^2} \approx \frac{n_1 - n_2}{n_1} \qquad \text{for } \Delta \ll 1 \tag{2.1}$$

Another parameter is the numerical aperture of a fiber. As one needs to couple light into the fiber from a surrounding media with refractive index n_0 (often air: $n_0 \approx 1$) and propagation inside the fiber is based on total internal reflection, the fiber can only guide light that enters under a curtain angle called the acceptance angle Θ_a:

The critical angle for total internal reflection (Θ_c) can be calculated using the law of reflection:

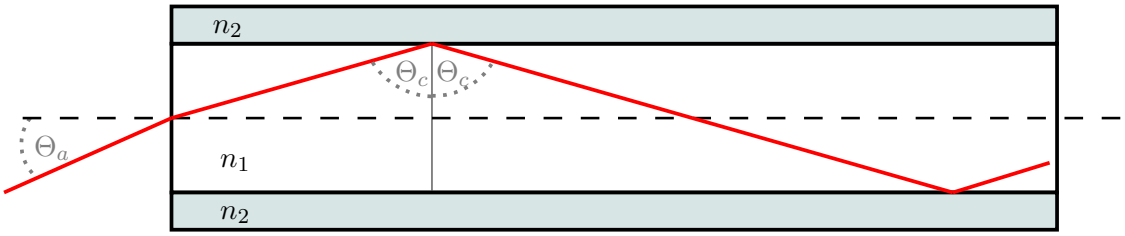

Figure 2: Total internal reflection and acceptance angle

$$\Theta_c = \arcsin(\frac{n_2}{n_1}) \tag{2.2}$$

From that the acceptance angle Θ_a can be calculated using geometry and the law of reflection once more:

$$n_0 \sin(\Theta_a) = n_1 \sin(90° - \Theta_c) = \sqrt{{n_1}^2 - {n_2}^2} = NA \tag{2.3}$$

The sine of the acceptance angle is in fiber optics often referred to as the numerical aperture (NA. Even this definition may only be valid for fibers with large core, like multi-mode fibers, because the ray optics used for the derivation will not hold for single-mode step-index fibers, manufacturers will state this parameter even for such fibers.

2.2. Fiber Modes

To solve the wave equation for optical fibers it is useful to attribute the cylindrical symmetry by expressing the wave equation in cylindrical coordinates (r,φ,z):

$$\frac{\partial^2 A}{\partial r^2} + \frac{1}{r}\frac{\partial A}{\partial r} + \frac{1}{r^2}\frac{\partial^2 A}{\partial \varphi^2} + \frac{\partial^2 A}{\partial z^2} + n^2 k_0^2 A = 0 \tag{2.4}$$

with A being a component of the electric or magnetic field and $k_0 = \omega/c = 2\pi/\lambda$. The equation can be solved by the method of separation of variables with the following ansatz and by replacing k with the propagation constant β:

$$A(r, \varphi, z) = R(r)\Phi(\varphi)e^{j\beta z} \tag{2.5}$$

For $\Phi(\varphi)$, the azimuthal function, the following equation is obtained:

$$\frac{d^2\Phi}{d\varphi^2} + l^2\Phi = 0 \tag{2.6}$$

with the solutions:

$$\Phi(\varphi) = \sin(l\varphi) \qquad \text{and} \qquad \Phi(\varphi) = \cos(l\varphi) \tag{2.7}$$

and l being an integer number such that $A(\varphi) = A(\varphi + 2\pi)$ and numbering different field distributions called modes as can be seen later.

For the radial component $R(r)$:

$$\frac{d^2R}{dr^2} + \frac{1}{r} + \left[n^2k_0^2 - \beta^2 - \frac{l^2}{r^2}\right]R = 0 \tag{2.8}$$

The refractive index of a fiber obvious depends on the radial position: $n = n(r)$. For a step-index fiber this relation can be expressed by defining the core and the cladding region:

$$n(r) = n_1 \qquad \text{for } r \leq a \qquad \text{and} \qquad n(r) = n_2 \qquad \text{for } n > a \tag{2.9}$$

with a being the core radius.

It is very useful to introduce some normalized variables at this point:

$$\rho = r/a \tag{2.10}$$

$$u = a\sqrt{n_1^2k_0^2 - \beta^2} \tag{2.11}$$

$$w = a\sqrt{\beta^2 - n_2^2k_0^2} \tag{2.12}$$

$$V = \sqrt{u^2 + w^2} = ak_0NA \tag{2.13}$$

V is the normalized frequency and will be a important design parameter. V can also be expressed by the wavelength λ and the refractive index difference Δ:

$$V = \frac{2\pi}{\lambda} aNA = \frac{2\pi}{\lambda} an_1\sqrt{2\Delta} \tag{2.14}$$

With this introduced, equation 2.8 for the two regions reads:

$$\frac{d^2R}{d\rho^2} + \frac{1}{\rho}\frac{dR}{d\rho} + (u^2 - \frac{l^2}{\rho^2})R = 0 \qquad \text{for } \rho \leq 1 \tag{2.15}$$

$$\frac{d^2R}{d\rho^2} + \frac{1}{\rho}\frac{dR}{d\rho} - (w^2 + \frac{l^2}{\rho^2})R = 0 \qquad \text{for } \rho > 1 \tag{2.16}$$

which solutions are Bessel functions:

$$R(\rho) = A_1 J_l(u\rho) \qquad \text{for } \rho \leq 1 \tag{2.17}$$

$$R(\rho) = A_2 K_l(w\rho) \qquad \text{for } \rho > 1 \tag{2.18}$$

Where J_l is a bessel function of the first kind and order l in the core region (Figure 3) and K_l is a modified bessel function of the second kind and order l in the cladding region (Figure 4).

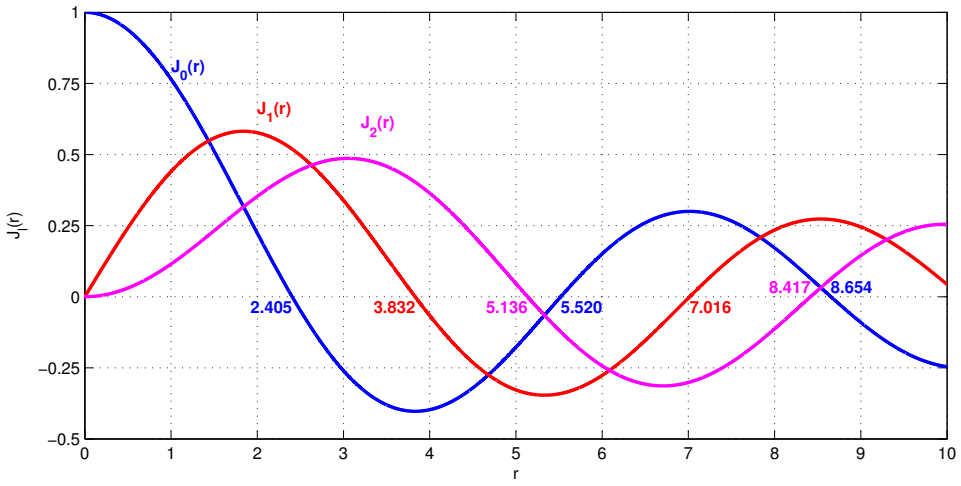

Figure 3: Plot of bessel function $J_l(r)$ of the first kind with orders $l = 0, 1, 2$ with zeros labelled

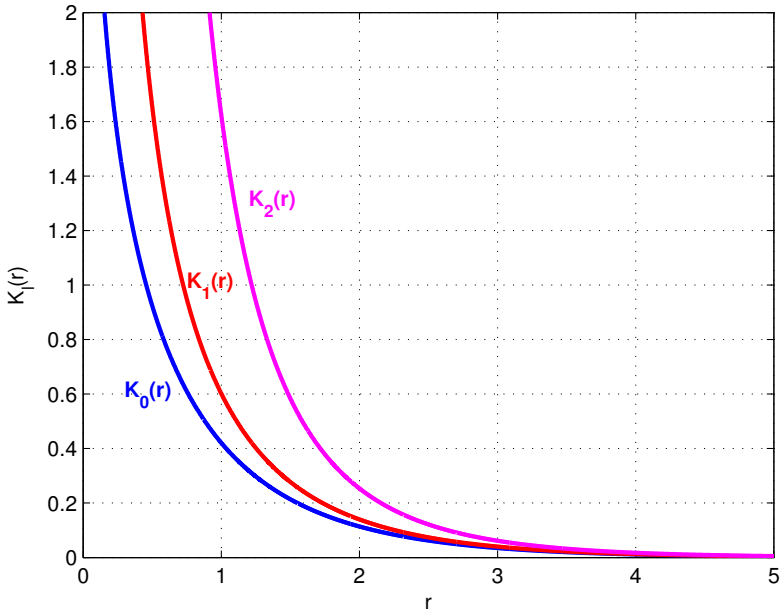

Figure 4: Plot of modified bessel function $K_l(r)$ of the second kind for orders $l = 0, 1, 2$

In the weak guidance approximation ($\Delta \ll 1$) the field matching conditions at the boundary require continuity of the transverse and tangential electric field components at the core – cladding interface ($\rho = 1$) with the following eigenvalue equation as solution [13]:

$$u\frac{J_{l\pm1}(u)}{J_l(u)} = \pm w\frac{K_{l\pm1}(w)}{K_l(w)} \tag{2.19}$$

For a given order l that equation can have multiple solutions m that result in different discrete propagation constants $\beta^{(lm)}$ with corresponding field distributions (modes) given by equation 2.5. The two indices l and m therefore characterize the modes. Equation 2.19 may be solved numerically and the solution can be seen in Figure 5:

One can see that below a certain frequency there is only a single mode, the fundamental mode, supported. That frequency is the cut-off frequency for the lowest higher order mode and at $V = V_c = 2.405$. As the normalized frequency V is related to the wavelength and the core diameter of the fiber through equation 2.14 one can easy realize if a fiber

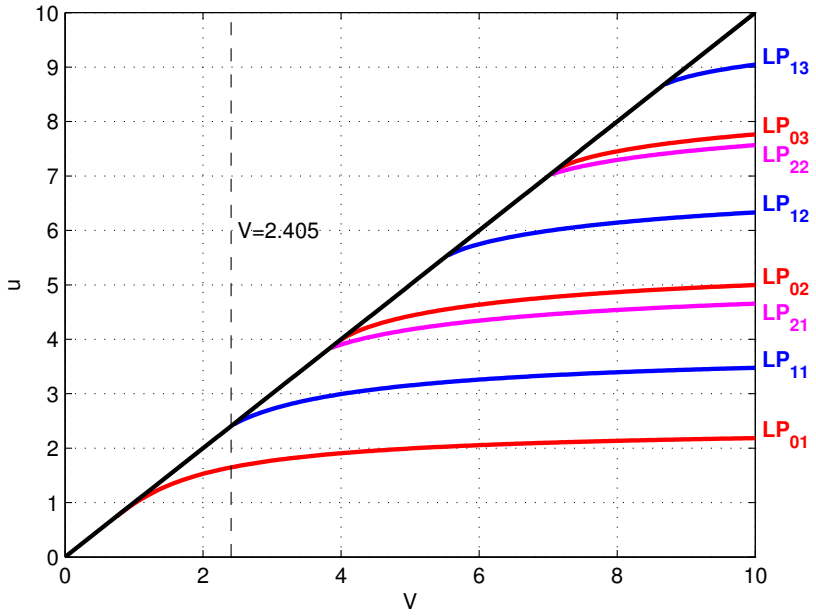

Figure 5: Solutions of equation 2.19 as a function of normalized frequency V

with given diameter is a single mode fiber or not.

$$b = 1 - \frac{u^2}{V^2} = \frac{(\beta/k)^2 - {n_2}^2}{{n_1}^2 - {n_2}^2} \tag{2.20}$$

Figure 6 shows the normalized propagation constant (b) defined by equation 2.20. The normalized propagation constant is defined such that if $\beta = n_2 k$, then the mode phase velocity is equal to the velocity of light in the cladding and therefore not guided, $b = 0$. As the mode is not guided by the fiber it is said to be cut-off. For $\beta > n_2 k$ the power gets more and more confined to the core until it reaches $\beta = n_1 k$, where the mode phase velocity matches the phase velocity of the core and $b = 1$.

2.3. Fiber Losses

As most fibers are manufactured from silica with additional doping to set the refractive index its the material absorption of silica that contribute to fiber losses and dispersion.

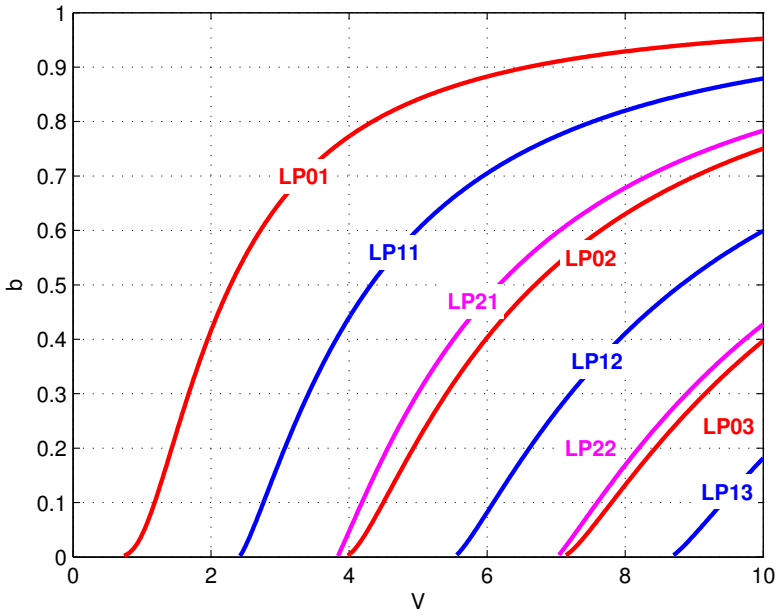

Figure 6: normalized propagation constant b in a step-index fiber

A typical parameter for fiber losses is the attenuation that is a logarithmic measure expressed in dB/km and defined by:

$$\alpha = \frac{10}{l} log\Big(\frac{P(0)}{P(l)}\Big) \tag{2.21}$$

with $P(0)$ being the launched optical power and $P(l)$ the power at the distance l.

Several mechanisms contribute to fiber losses that are wavelength dependent: Below $1.2\mu m$ the Rayleigh scattering which arises from density fluctuation frozen in while manufacturing the fiber [12]. In the wavelength region from $1.2\mu m$ to $1.5\mu m$ the absorption due to OH-ions dominates. The OH-ion has a fundamental vibrational absorption peak near $2.73\mu m$ and overtones around $1.23\mu m$ and a dominant peak at about $1.4\mu m$.

With special precautions taken during manufacturing the absorption peak at $1.4\mu m$ can be reduced below $0.5dB/km$ [12]. At wavelengths above $1.6\mu m$ infrared absorption contributes most. The Rayleigh scattering is an intrinsic loss and therefore sets the ultimate limit on fibers and scales with λ^{-4} [12]. The loss mechanisms are summarized

in Figure 7.

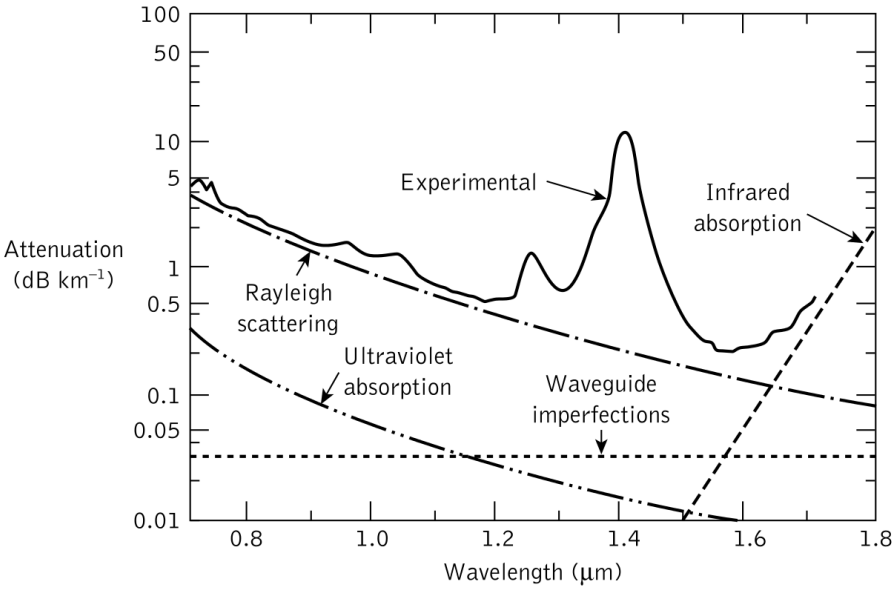

Figure 7: Attenuation spectrum for single-mode fiber [13]

2.4. Fiber Dispersion

There are two major dispersion mechanism related to fiber propagation: mode dispersion and chromatic dispersion (material dispersion and waveguide dispersion). Mode dispersion arises when multiple modes propagate in a waveguide. As can be seen in Figure 6, that for a given normalized frequency V, the propagation constant differs for different modes. A pulse transmitted in a multimode fiber will therefore be stretched according to the transmission time of the slowest and fastest mode. Thus mode dispersion can be avoided using single-mode fibers.

Chromatic dispersion is the combination of material dispersion and waveguide dispersion and results from the finite spectral linewidth of optical sources or the spectral bandwidth of pulses. Within that bandwidth each frequency may experience a different speed due to variations in the refractive index of the media.

Waveguide dispersion is obtained when calculating the effective refractive index of a

waveguide for example out of the normalized propagation constant. Figure 6 therefore gives a qualitative picture of the effective refractive index that will range from n_2 if $b = 0$ to n_1 if $b = 1$. The waveguide dispersion is negative (with respect to λ) over the total single mode range ($V_c < 2.405$) for standard step-index fibers.

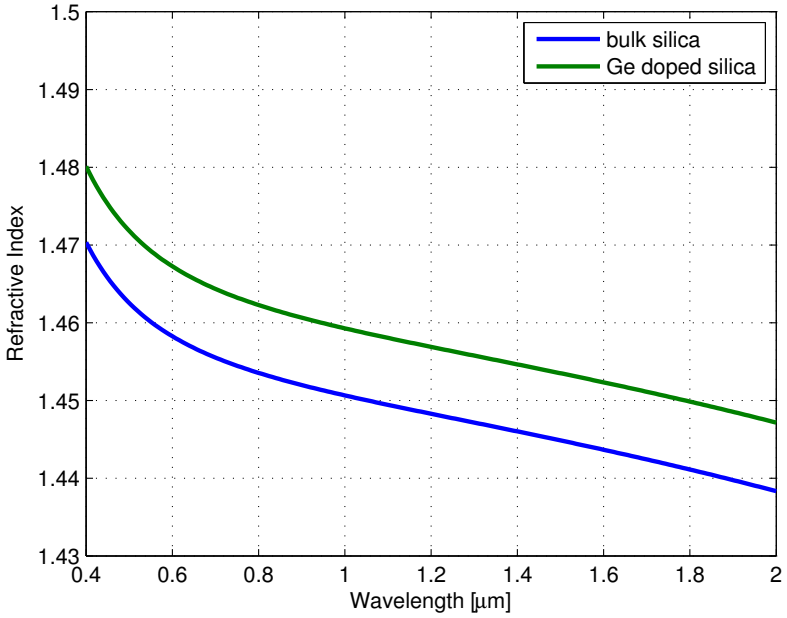

Figure 8: Refractive Index of bulk silica and Ge doped silica

Material dispersion is the dispersion that arises from the material property that the refractive index depends on the wavelength of the light (see Figure 8). A taylor expansion of the propagation constant β around a center frequency ω_0 gives:

$$\beta(\omega) = n(\omega)\frac{\omega}{c} = \beta_0 + \beta_1(\omega - \omega_0) + \frac{1}{2}\beta_2(\omega - \omega_0)^2 + ... \tag{2.22}$$

β_1 is the inverse of the group velocity (v_g) and defined by:

$$\beta_1 = \frac{d\beta}{d\omega} = \frac{1}{v_g} = \frac{1}{c}\Big(n + \omega\frac{dn}{d\omega}\Big) = \frac{1}{c}\Big(n - \lambda\frac{dn}{d\lambda}\Big) \tag{2.23}$$

where c is the speed of light.

$\beta_2 = d/d\omega(\beta_1)$ is the change of group velocity with respect to ω. This change is called group velocity dispersion (GVD) and is a major source of pulse broadening in fiber systems:

$$\beta_2 = \frac{d}{d\omega}\beta_1 = \frac{d}{d\omega}\left(\frac{1}{v_g}\right) = \frac{1}{c}\left[2\frac{dn}{d\omega} + \omega\frac{d^2n}{d\omega^2}\right] \tag{2.24}$$

The dispersion parameter D_λ is then defined as:

$$D_\lambda = \frac{d}{d\lambda}\left(\frac{1}{v_g}\right) = -\frac{\lambda}{c}\frac{d^2n}{d\lambda^2} \tag{2.25}$$

The material dispersion for fused silica shows a strong wavelength dependence and changes its sign after passing zero dispersion at about $1.27\mu m$ for bulk silica (used as cladding) or at about $1.31\mu m$ for standard germanium doped silica (used as core). Figure 9 shows the chromatic dispersion for a step index fiber.

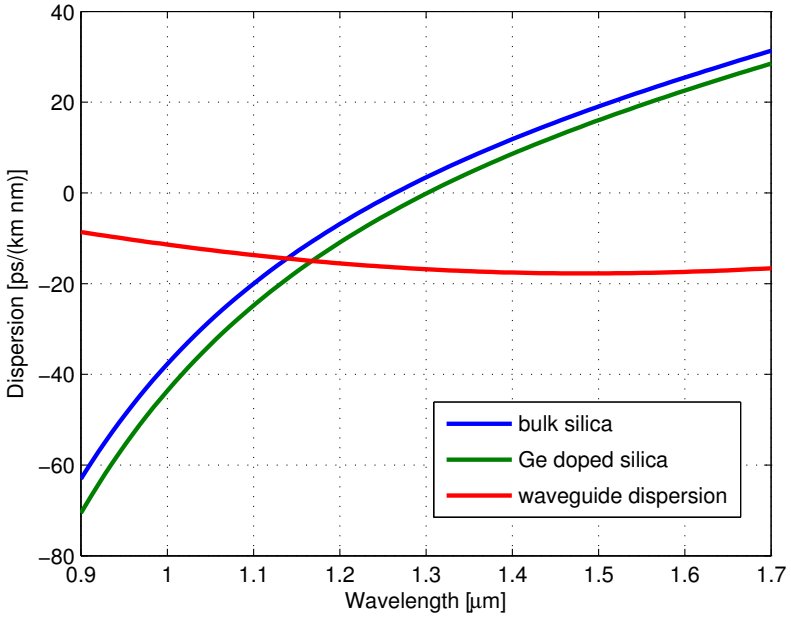

Figure 9: Chromatic Dispersion for step-index silica fiber

2.5. Fiber Handling

The process of joining two fiber ends is known as splicing. Before two fiber ends can be joined together the fiber ends have to be prepared. First all protective coatings need to be removed which is referred to as "stripping". After cleaning the now bare fiber the fibers ends need to be prepared, a process called "cleaving".

The term "cleave" is defined[1] as:

> In an optical fiber, a deliberate, controlled break, intended to create a perfectly flat endface, perpendicular to the longitudinal axis of the fiber. Note: A cleave is made by first introducing a microscopic fracture ("nick") into the fiber with a special tool, called a "cleaving tool,"which has a sharp blade of hard material, such as diamond, sapphire, or tungsten carbide. If proper tension is applied to the fiber as the nick is made, or immediately afterward (this may be done by the cleaving tool in some designs, or manually in other designs), the fracture will propagate in a controlled fashion, creating the desired endface.

It is important for the quality of the splice to have a clean, flat and not angled surface as those factors directly influence the splicing losses.

The act of joining two fiber ends using localized heat is known as fusion splicing and a common technique to create permanent connection. The prepared fiber ends are then aligned and fused or melted using an electric spark (or another heat source like a gas flame or lasers). The goal of this process is to create a permanent connection that does not alter the fibers properties, as if the fiber was never broken there. The process of aligning and fusing the fibers is often automated as tolerances within the wavelength of light cause high splicing loses or disturbance of the fiber modes.

In automated systems there usually is also some way to estimate the splice losses. By analyzing the passing through and reflected light at the splice position the quality of the connection can be estimated. For polarization maintaining (PM) fibers it is not

[1] ATIS Telecom Glossary 2000 T1.523-2001

sufficient to align the fiber in plane but also to match the polarization profile by rotating the fibers.

After splicing the splice needs to be protected by using splice protectors or re-coating the fiber. This increases the mechanical stability of the splice. In the case of re-coating the protective buffer is restored.

3. Pulse Propagation in Optical Fiber

The key to femtosecond lasers is the understanding of how pulses are formed and propagate in the optical medium. Modelocking is a group of techniques able to produce ultra short pulses down to the femtosecond regime. The name modelocking refers to the underlying method of generating multiple modes with a fixed (locked) phase. When a pulse propagates in an optical medium it will experience several interactions like dispersive or nonlinear effects.

3.1. Nonlinear Pulse Propagation

As a starting point to analyze nonlinear pulse propagation the wave equation, as obtained by Maxwell's equations, is a good choice:

$$\nabla^2 \boldsymbol{E} - \frac{1}{c^2}\frac{\partial^2 \boldsymbol{E}}{\partial t^2} = \mu_0 \frac{\partial^2 \boldsymbol{P}}{\partial t^2} \tag{3.1}$$

Where $\boldsymbol{E}$ is the electric field, $\boldsymbol{P}$ the induced polarization, c the speed of light and μ_0 the vacuum permeability.

Polarization is defined as the media response to the electric field, which is expressed by the susceptibility χ and the vacuum permittivity ϵ_0:

$$\boldsymbol{P} = \epsilon_0 \boldsymbol{\chi} \boldsymbol{E} \tag{3.2}$$

When intense electromagnetic fields are considered this response becomes nonlinear and depends on the strength of the field:

$$\boldsymbol{\chi}(\boldsymbol{E}) = \chi^{(1)} + \chi^{(2)}\boldsymbol{E} + \chi^{(3)}\boldsymbol{E}\boldsymbol{E} + ... \tag{3.3}$$

The total polarization, attributing that the susceptibility is a tensor and using the Einstein notation, reads as:

$$P_i = \epsilon_0 \chi^{(1)}_{ij} E_j + \epsilon_0 \chi^{(2)}_{ijk} E_j E_k + \epsilon_0 \chi^{(3)}_{ijkl} E_j E_k E_l + ... \tag{3.4}$$

For inversion symmetric materials, like silica fibers, no susceptibilities of even order exist and the contribution of orders greater than 4 are very weak. So only the linear susceptibility $\chi^{(1)}$ and the third order susceptibility $\chi^{(3)}$ are to be considered. Therefore the polarization is often expressed as:

$$\boldsymbol{P} = \boldsymbol{P}_L + \boldsymbol{P}_{\mathrm{NL}} \tag{3.5}$$

which splits the polarization into a linear ($\boldsymbol{P}_L$) and a nonlinear ($\boldsymbol{P}_{\mathrm{NL}}$) term. Equation 3.1 therefore reads:

$$\nabla^2 \boldsymbol{E} - \frac{1}{c^2}\frac{\partial^2 \boldsymbol{E}}{\partial t^2} = \mu_0 \frac{\partial^2 \boldsymbol{P}_L}{\partial t^2} + \mu_0 \frac{\partial^2 \boldsymbol{P}_{\mathrm{NL}}}{\partial t^2} \tag{3.6}$$

With $\boldsymbol{P}_L$ being linear dependent on the electric field one can express it in term of the electric field:

$$\epsilon_0 \boldsymbol{E} + \boldsymbol{P}_L = \epsilon_0 \epsilon \boldsymbol{E} \tag{3.7}$$

The nonlinear polarization now appears as a source term in the wave equation 3.6:

$$\nabla^2 \boldsymbol{E} - \frac{\epsilon}{c^2}\frac{\partial^2 \boldsymbol{E}}{\partial t^2} = \mu_0 \frac{\partial^2 \boldsymbol{P}_{\mathrm{NL}}}{\partial t^2} \tag{3.8}$$

To solve this equation some approximations must be made [12]: $\boldsymbol{P}_{\mathrm{NL}}$ is assumed to be a small perturbation to $\boldsymbol{P}_L$, the field is assumed to be monochromatic and linearly polarized while the polarization is maintained along the fiber and that the media response is instantaneous e.g. that the Raman-effect and self steepening can be neglected.

Such an electric field, linearly polarized in the x direction, can be expressed using the slowly varying envelope approximation:

$$E(t) = \frac{1}{2}\hat{x}\left[\tilde{E}(\omega)\exp(j\omega t) + c.c.\right] \tag{3.9}$$

Recalling equation 3.4 with the components of the electric field only in one direction ($i = j = k = 1 \stackrel{\wedge}{=} x$) and therefore $E_{2,3} = 0$ simplifies as:

$$P_1(t) = \epsilon_0 \chi_{11}^{(1)} E_1(t) + \epsilon_0 \chi_{1111}^{(3)} E_1(t) E_1(t) E_1(t) \tag{3.10}$$

as there are no other directions other than the x direction we can reduce this to:

$$P_L(t) = \epsilon_0 \chi^{(1)} E(t) \tag{3.11}$$

$$P_{\mathrm{NL}}(t) = \epsilon_0 \chi^{(3)} E^3(t) \tag{3.12}$$

and the nonlinear polarization results in:

$$\begin{aligned} P_{\mathrm{NL}}(t) = \frac{1}{2}\epsilon_0 \chi^{(3)} \Big\{ & \\ & \Big[\frac{1}{4}\tilde{E}(\omega)\tilde{E}(\omega)\tilde{E}(\omega)\exp(j3\omega t) + c.c\Big] + \\ & \Big[\frac{3}{4}\tilde{E}(\omega)\tilde{E}(\omega)\tilde{E}^*(\omega)\exp(j\omega t) + c.c\Big] \\ \Big\} & \end{aligned} \tag{3.13}$$

where one can identify components at the fundamental frequency and at the third harmonic:

$$\tilde{P}_{\mathrm{NL}}(\omega) = \frac{3}{4}\epsilon_0 \chi^{(3)} \tilde{E}(\omega)\tilde{E}(\omega)\tilde{E}^*(\omega) \tag{3.14}$$

$$\tilde{P}_{\mathrm{NL}}(3\omega) = \frac{1}{4}\epsilon_0 \chi^{(3)} \tilde{E}(\omega)\tilde{E}(\omega)\tilde{E}(\omega) \tag{3.15}$$

The third harmonic term can lead to a field at three times the fundamental frequency if an effort is taken to achieve phase matching of the two fields. Furthermore if a superposition of fields at different frequencies is launched, sum and difference frequencies can be observed. As in general phase matching does not occur in optical fibers that term can be neglected.

The term at the fundamental frequency gives rise to the optical Kerr-effect: the refractive index of the medium depends on the intensity of the local electric field.

The total polarization at the frequency ω:

$$\tilde{P}(\omega) = \epsilon_0 \chi^{(1)} \tilde{E}(\omega) + \frac{3}{4} \epsilon_0 \chi^{(3)} \tilde{E}(\omega) \tilde{E}(\omega) \tilde{E}^*(\omega) \tag{3.16}$$

With the intensity defined as $I = n_0 \tilde{E} \tilde{E}^* / 2 Z_0$ where Z_0 is the vacuum impedance:

$$\tilde{P}(\omega) = \epsilon_0 \big[\chi^{(1)} + \frac{3 \chi^{(3)} Z_0}{2 n_0} I \big] \tilde{E}(\omega) = \epsilon_0 [\chi_0 + \Delta\chi(I)] \tilde{E}(\omega) \tag{3.17}$$

The effective susceptibility of the media depends on the intensity. With $\epsilon = 1 + \chi$ and $n = \sqrt{\mathrm{Re}(\epsilon)}$ and using the Taylor expansion of the square root:

$$n = \sqrt{\mathrm{Re}(1+\chi)} = \sqrt{1 + \chi_0 + \Delta\chi(I)} \approx n_0 + \frac{1}{2 n_0} \Delta\chi(I) \tag{3.18}$$

the third order nonlinearity translates into a intensity dependent refractive index:

$$n = n_0 + n_2 I \tag{3.19}$$

$$n_2 := \frac{3 Z_0}{2 n_0^2} \chi^{(3)} \tag{3.20}$$

This change of the refractive index results in a change of the phase velocity and a modulation of the phase of the pulse. Therefore this effect is called self phase modulation (SPM).

This effect can also occur when fields at different frequencies are involved and is then called cross phase modulation (XPM).

Using the above made assumptions one can translate the wave equation into the nonlinear Schrödinger Equation which also accounts for the physical properties of fibers and therefore includes fiber modes.

3.2. Nonlinear Schrödinger Equation

Pulses propagating in a fiber can be described by the nonlinear Schrödinger Equation (NLSE) [12]:

$$\frac{\partial A}{\partial z} + \frac{\alpha}{2} A + j \frac{\beta_2}{2} \frac{\partial^2 A}{\partial t^2} - \frac{\beta_3}{6} \frac{\partial^3 A}{\partial t^3} = j\gamma \Big[|A|^2 A + \frac{j}{\omega_0} \frac{\partial}{\partial t} (|A|^2 A) - T_R A \frac{\partial |A|^2}{\partial t} \Big] \tag{3.21}$$

In Equation (3.21) $A(z,t)$ is a slowly varying envelope function propagating in a reference frame with the group velocity along the z direction in a third order nonlinear medium, like silica fiber, and α contributes to the linear loss or gain. Higher order nonlinearities can be neglected due to their weak contribution in silica fibers.

β_2 and β_3 are the dispersion coefficients as obtained by a Taylor expansion of the frequency dependent propagation constant $\beta(\omega)$ around a carrier frequency ω_0:

$$\beta(\omega) = \beta_0 + \beta_1(\omega - \omega_0) + \frac{1}{2}\beta_2(\omega - \omega_0)^2 + \frac{1}{6}\beta_3(\omega - \omega_0)^3 + \dots \tag{3.22}$$

β_1 is the inverse of the group velocity:

$$\beta_1 = \frac{1}{v_g} \tag{3.23}$$

and β_2 is the derivative of β_1 with respect to ω:

$$\beta_2 = \frac{d}{d\omega}\left[\frac{1}{v_g}\right] \tag{3.24}$$

and is therefore called group velocity dispersion (GVD) and β_3 third order dispersion (TOD) . Higher orders have been neglected in equation (3.21) because of their weak contribution.

γ is referred to as the nonlinearity coefficient and defined by:

$$\gamma = \frac{\omega_0 n_2}{c_0 A_{\text{eff}}} \tag{3.25}$$

where n_2 is the nonlinear refractive index and responsible for self phase modulation, c_0 the speed of light and A_{eff} the effective mode area.

The term $\frac{j}{\omega_0}\frac{\partial}{\partial t}(|A|^2 A)$ accounts for self-steepening while $T_R A\frac{\partial |A|^2}{\partial t}$ accounts for Raman nonlinearities and are shown here for completeness.

3.3. Group Velocity Dispersion

Group Velocity Dispersion is the dominant source of temporal broadening of pulses in an optical medium.

To analyse dispersive effects on pulse propagation we can use equation (3.21) and skip the nonlinear terms. To simplify the equation further, losses and third order dispersion are neglected as well:

$$\frac{\partial A}{\partial z} + j\frac{\beta_2}{2}\frac{\partial^2 A}{\partial t^2} = 0 \tag{3.26}$$

To solve that equation a Fourier transformation gives ($\frac{\partial^2}{\partial t^2} \rightarrow (j\omega)^2 = -\omega^2$):

$$\frac{\partial \tilde{A}}{\partial z} = j\frac{\beta_2}{2}\omega^2 \tilde{A} \tag{3.27}$$

with $\tilde{A}(z,\omega)$ is the Fourier transform of $A(z,t)$ this leads to the solution:

$$\tilde{A}(z,w) = \tilde{A}(0,w)\exp(j\frac{\beta_2}{2}\omega^2 z) \tag{3.28}$$

with $\tilde{A}(0,w)$ being the Fourier transformed pulse shape at $z = 0$.

For a Gaussian pulse one obtains:

$$A(0,t) = A_0\exp(\frac{-t^2}{2t_0^2}) \tag{3.29}$$

$$\tilde{A}(0,w) = \int_{-\infty}^{\infty} A(0,t)\exp(i\omega t)dt = A_0\sqrt{2\pi t_0^2}\exp(-\frac{t_0^2\omega^2}{2}) \tag{3.30}$$

Plugging the pulse spectrum (3.30) into equation (3.28) gives the pulse spectrum after propagating the distance z:

$$\tilde{A}(z,\omega) = A_0\sqrt{2\pi t_0^2}\exp(-\frac{t_0^2\omega^2}{2})\exp(j\frac{\beta_2}{2}\omega^2 z) \tag{3.31}$$

With $\exp(j\frac{\beta_2}{2}\omega^2 z)$ being a quadratic phase shift the pulse accumulates during propagation. The amplitude spectrum itself stays unchanged. To obtain the pulse shape in time domain the inverse Fourier transformation of equation (3.31) is taken:

$$
\begin{aligned}
A(z,t) &= \frac{1}{2\pi}\int_{-\infty}^{\infty}\tilde{A}(z,\omega)\exp(-j\omega t)d\omega \\
&= \frac{A_0 t_0}{\sqrt{2\pi}}\int_{-\infty}^{\infty}\exp\Big(-\Big[\omega^2\Big(\frac{t_0^2 - j\beta_2 z}{2}\Big) + j\omega t\Big]\Big)d\omega \\
&= A_0\frac{t_0}{\sqrt{t_0^2 - j\beta_2 z}}\exp\Big(-\frac{t^2}{2(t_0^2 - j\beta_2 z)}\Big)
\end{aligned}
\tag{3.32}
$$

Equation (3.32) clearly shows that the pulse width, amplitude and phase are changed due to GVD. A measure to estimate if dispersion needs to be considered is the dispersion length L_D:

$$
L_D = \frac{t_0^2}{|\beta_2|} \tag{3.33}
$$

After the pulse traveled the length of L_D the pulse width is increased by a factor of $\sqrt{2}$ [12].

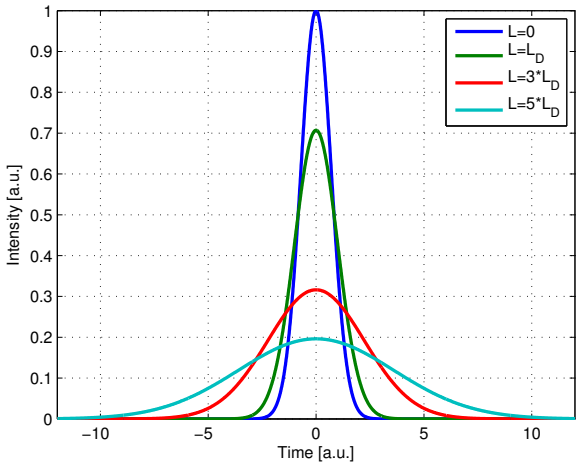

Figure 10: GVD broadened pulse

3.4. Self Phase Modulation

When assuming no dispersion and no loss the effect of self phase modulation can be studied:

$$\frac{\partial A}{\partial z} = j\gamma|A|^2 A \tag{3.34}$$

As one expects a phase shift to be introduced the following ansatz will solve this equation:

$$A(z,t) = A_0(z,t)\exp(-j\Phi(z,t)) \tag{3.35}$$

$$\frac{\partial A_0(z,t)}{\partial z}\exp(-j\Phi(z,t)) + A_0(z,t)\exp(-j\Phi(z,t))(-j)\frac{\partial \Phi(z,t)}{\partial z} = j\gamma|A|^2 A_0(z,t)\exp(-j\Phi(z,t)) \tag{3.36}$$

By comparing the terms the following two equations are obtained:

$$\frac{\partial A_0(z,t)}{\partial z} = 0 \tag{3.37}$$

$$\frac{\partial \Phi(z,t)}{\partial z} = -\gamma|A(z,t)|^2 \tag{3.38}$$

Equation (3.37) implies that the pulse envelope is independent of the propagation distance z while equation (3.38) can be integrated to obtain the solution:

$$A(z,t) = A(0,t)\exp(-j\gamma|A|^2 z) \tag{3.39}$$

For a Gaussian pulse $A(z,t) = A_0\exp(-t^2/t_0^2)$ the induced frequency chirp, while introducing the nonlinear length $L_{\mathrm{NL}} = 1/(\gamma|A_0|^2)$, can be calculated as

$$\Delta\omega(t) = \frac{\partial \Phi(z,t)}{\partial t} = \frac{\partial}{\partial t}(-\gamma|A|^2 z) = \frac{4t}{t_0^2}\frac{z}{L_{\mathrm{NL}}}\exp(-2t^2/t_0^2) \tag{3.40}$$

3.5. Higher Order Dispersion and Combined Effects

When trying to analyze higher order dispersive effects or propagation with SPM and GVD analytical solutions are difficult to obtain. Recalling equation (3.21):

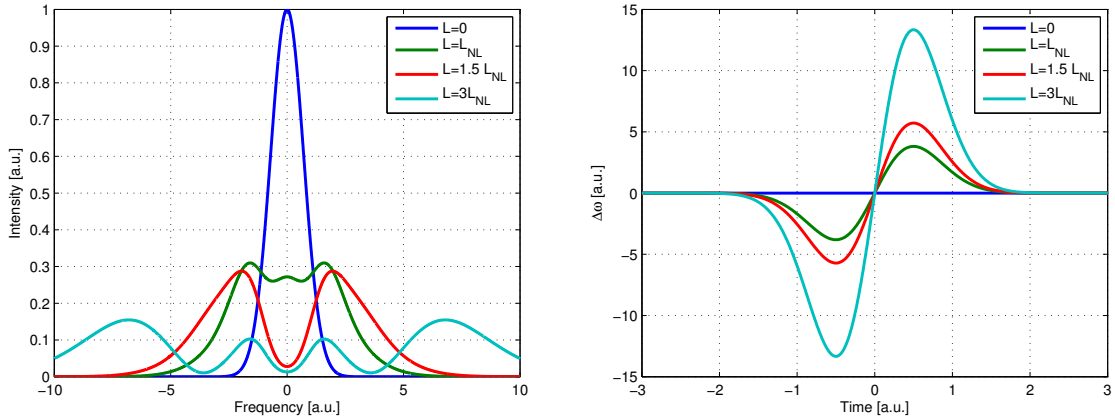

Figure 11: SPM broadened Spectrum and Frequency Chirp

$$\frac{\partial A}{\partial z} + \frac{\alpha}{2}A + j\frac{\beta_2}{2}\frac{\partial^2 A}{\partial t^2} - \frac{\beta_3}{6}\frac{\partial^3 A}{\partial t^3} = j\gamma\Big[|A|^2 A + \frac{j}{\omega_0}\frac{\partial}{\partial t}(|A|^2 A) - T_R A\frac{\partial |A|^2}{\partial t}\Big]$$

One way to solve the equation numerically is the Split Step Fourier Method (SSFM):

$$\frac{\partial A}{\partial z} = (\hat{D} + \hat{N})A \tag{3.41}$$

$\hat{D}$ is the differential operator that introduces dispersion and loss or gain:

$$\hat{D} = \frac{\alpha}{2} + j\frac{\beta_2}{2}\frac{\partial^2}{\partial t^2} - \frac{\beta_3}{6}\frac{\partial^3}{\partial t^3} \tag{3.42}$$

where $\hat{N}$ accounts for nonlinearities:

$$\hat{N} = j\gamma\Big[|A|^2 + \frac{j}{\omega_0}\frac{1}{A}\frac{\partial}{\partial t}(|A|^2 A) - T_R\frac{\partial |A|^2}{\partial t}\Big] \tag{3.43}$$

The idea of the SSFM is to separate propagation into 2 steps: a dispersive only step and a pure nonlinear step. Naturally, when propagating, dispersion and nonlinearities act together on the pulse, but when choosing the step size small enough the result obtained using SSFM is comparable.

Approximating equation (3.41) and separating the operators one obtains:

$$A(z+h,t) = \exp(h\hat{D})\exp(h\hat{N})A(z,t) \tag{3.44}$$

$\exp(h\hat{D})$ can be evaluated in the frequency domain, where the FFT algorithm provides a fast and efficient way to perform the transformation. $D(j\omega)$ is obtained directly from equation (3.42) by replacing time derivatives by: $\partial^n/\partial t^n \rightarrow (j\omega)^n$:

$$\hat{D}(j\omega) = -\frac{\alpha}{2} - j\frac{\beta_2}{2}(j\omega)^2 + \frac{\beta_3}{6}(j\omega)^3 \tag{3.45}$$

The first step can be solved by:

$$\exp(h\hat{D})A(z,t) = \mathrm{FFT}^{-1}\Big[\exp(h\hat{D}(j\omega))\,\mathrm{FFT}[A(z,t)]\Big] \tag{3.46}$$

The nonlinear step must be solved in an iterative way, but the implementation of the algorithm is straightforward.

Figure 12, 13 and 14 show simulation results using SSFM with $L_{\mathrm{NL}} = L_D$.

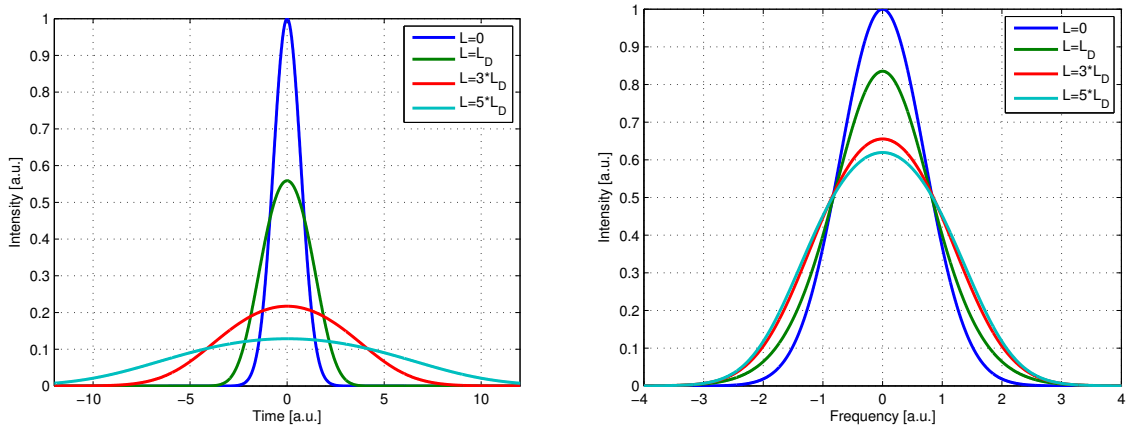

Figure 12: SSFM: pulse evolution with GVD and SPM

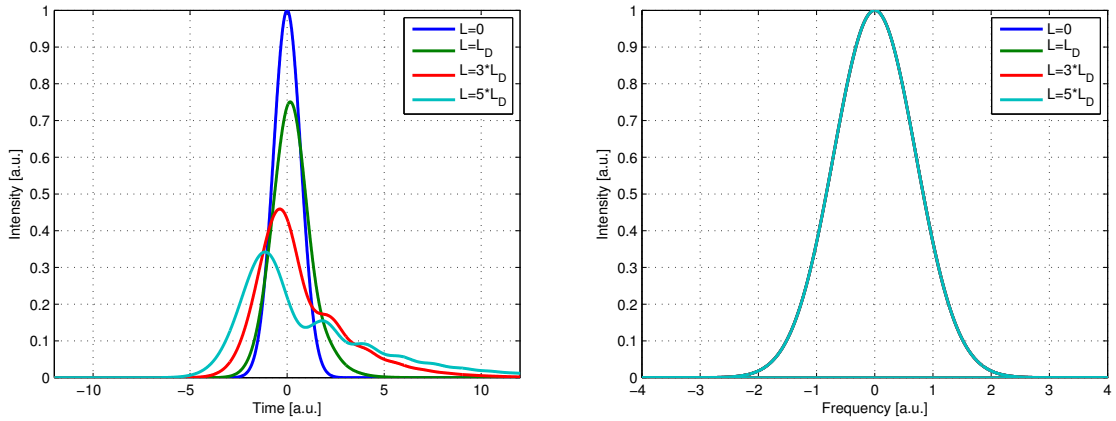

Figure 13: SSFM: pulse evolution with GVD and TOD

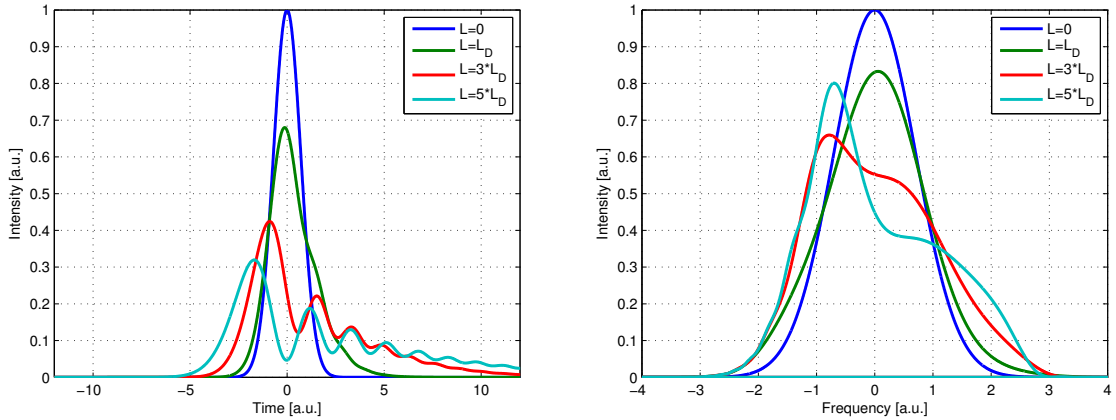

Figure 14: SSFM: pulse evolution with GVD, TOD and SPM

3.6. Nonlinear Polarization Evolution

For obtaining the nonlinear Schrödinger Equation one assumption made was that the polarization state of the incident light is preserved during the propagation along the fiber. As this is not the case in general this assumption will be dropped here.

Even if a fiber only transmits the fundamental mode and is therefore called single mode fiber (SMF) the fiber support two modes of orthogonal polarization, due to symmetry. For ideal fibers, with perfectly cylindrical geometry, those modes have the same propagation constants ($n_x = n_y$, when assuming propagation in z direction) and are called degenerated [12].

But due to limitations in manufacturing perfectly shaped fibers and anisotropic stress inside the fiber, all fiber suffer from modal birefringence ($n_x \neq n_y$). As a measure the degree of model birefringence B_m is defined as the refractive index mismatch:

$$B_m = |n_x - n_y| \tag{3.47}$$

In normal single mode fibers B_m and the orientation of the x and y axes change randomly and lead to polarization mode dispersion. By incorporating a stronger refractive index difference, while manufacturing the fiber, that is stronger in magnitude than the random changes, such fibers have nearly constant birefringence and offer two principal axes along which the incident state of polarization is preserved during propagation. Such fibers are called polarization-maintaining fibers.

The two axes are identified as the slow and fast axes where slow and fast refer to the phase velocity of the wave in that direction. With $n_x > n_y$ and the definition of phase velocity $v_{ph} = c_0/n$ one calls x the slow axis and y the fast axis.

When constant birefringence is assumed and linearly polarized light is launched at an angle with respect to one of the axes the state of polarization will change and become elliptical. From elliptical it will change to circular, from circular to elliptical and back to linear in a periodic manner, as illustrated in Figure 15.

That period is the beat length and defined by:

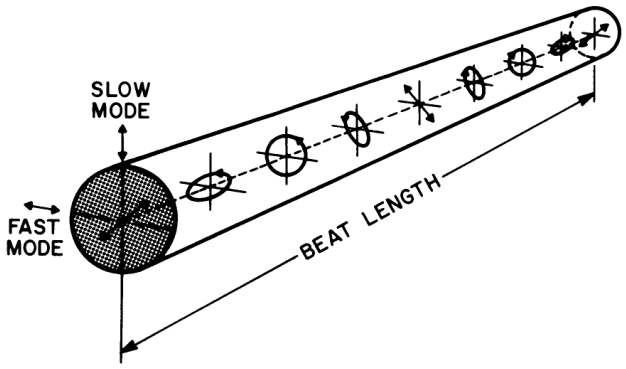

Figure 15: Polarization Mode Dispersion, Beat Length [12]

$$L_B = \frac{\lambda}{B_m} \tag{3.48}$$

The beat length can range from $1cm$ for high birefringence fiber up to several meters for low birefringence fiber.

When including nonlinear effects like the optical Kerr-effect the refractive index is depending on the intensity and so even perfectly manufactured fiber would become birefringent.

The electric field of an arbitrary polarized optical wave can be written as:

$$\boldsymbol{E}(\boldsymbol{r},t) = \frac{1}{2}(\boldsymbol{x}E_x + \boldsymbol{y}E_y)\exp(-j\omega_0 t) + c.c. \tag{3.49}$$

Recalling equation 3.4 for the polarization and accounting only for the third order parts at the fundamental frequency and using tensor rules for symmetric and isotropic media [12]:

$$P_x = \frac{3\epsilon_0}{4}\chi^{(3)}_{xxxx}\left[\left(|E_x|^2 + \frac{2}{3}|E_y|^2\right)E_x + \frac{1}{3}(E_x^* E_y)E_y\right] \tag{3.50}$$

$$P_y = \frac{3\epsilon_0}{4}\chi^{(3)}_{xxxx}\left[\left(|E_y|^2 + \frac{2}{3}|E_x|^2\right)E_y + \frac{1}{3}(E_y^* E_x)E_x\right] \tag{3.51}$$

with the total nonlinear polarization as:

$$\boldsymbol{P}_{\mathrm{NL}} = \frac{1}{2}(\boldsymbol{x}P_x + \boldsymbol{y}P_y)\exp(-j\omega_0 t) + c.c \tag{3.52}$$

The main contribution to the refractive index change in the x direction (n_x) in the equation for P_x comes from the term proportional to E_x and can be written as:

$$\Delta n_x = n_2\Big(|E_x|^2 + \frac{2}{3}|E_y|^2\Big) \tag{3.53}$$

The term proportional to $|E_x|^2$, the intensity in the x direction, is responsible for self phase modulation while the second part results in cross phase modulation because the change in refractive index, and therefore the nonlinear phase shift depends on the intensity of the other polarization component and induces a nonlinear coupling between these components.

The refractive index change in the y direction is expressed in an analog manner:

$$\Delta n_y = n_2\Big(|E_y|^2 + \frac{2}{3}|E_x|^2\Big) \tag{3.54}$$

For circular polarized light the intensities $|E_x|^2$ and $|E_y|^2$ are of same magnitude and no cross phase modulation occurs. For elliptical polarized light the nonlinear phase shift induced by the orthogonal component results in a rotation of the polarization ellipse; an effect called nonlinear polarization rotation. Together with some polarization optics this effect can serve as a fast passive modelocking mechanism [14].

3.7. Ultrafast Pulse Characterization

The main problem of characterizing ultrafast pulses is that they are ultrafast. Electro-optical devices like photodiodes are several orders of magnitude slower and therefore fail to measure femtosecond pulse duration or the phase of ultrashort pulses. An ultrashort optical pulse can be fully described by its time dependent intensity and phase:

$$E(t) = \frac{1}{2}\sqrt{(I(t))}\exp(i[\omega_0 t - \Phi(t)]) + c.c. \tag{3.55}$$

So to fully characterize a pulse both informations are mandatory.

A technique allowing to retrieve the complete time dependent intensity and phase of a ultrashort pulse is frequency-resolved optical gating (FROG). The basis of FROG is a nonlinear autocorrelator which output signal is analyzed by a spectrometer. There are different nonlinearities that can be exploited but second harmonic generation offers some advantages over others. A simplified setup for a SH FROG (second harmonic FROG) can be seen in Figure 16.

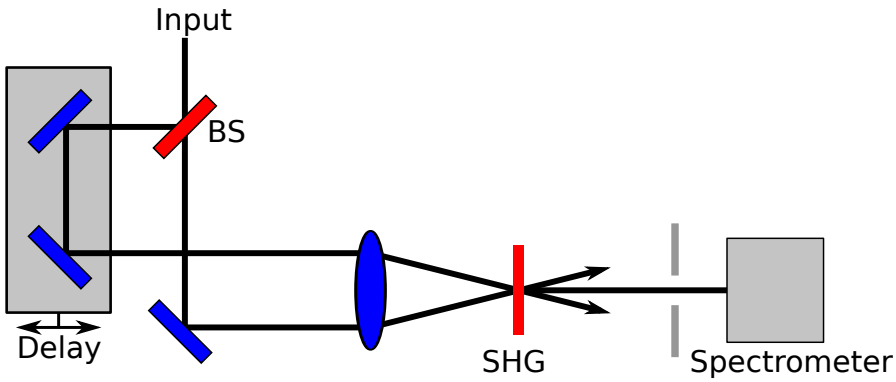

Figure 16: SH FROG Setup: SHG - second harmonic generation crystal, BS - beam splitter

The output recorded by the spectrometer is given by

$$I_{FROG}(\omega,\tau) = \left| \int_{-\infty}^{\infty} E(t)E(t-\tau)\exp(i\omega t)\,dt \right|^2 \tag{3.56}$$

and is a 2D time frequency plot. That data must then be processed using an iterative phase retrieval algorithm to obtain the time dependent intensity and phase of the pulse.

4. All-Normal Dispersion (ANDi) Femtosecond Fiber Laser

4.1. Introduction

The most important physical processes in a passively modelocked femtosecond laser are linear group-velocity dispersion, nonlinear phase accumulation through self-phase modulation and amplitude modulation produced by a saturable absorber [1].

Modelocking (ML) is a class of techniques that allow the generation of ultrashort pulses. This is achieved by synchronizing the phase of multiple longitudinal modes in such a way that the modes interfere constructive in a periodic manner at a given time. This can be done by modulating the loss of a laser cavity either active (active modelocking) or passive (passive modelocking). Generally, the shortest pulses can be obtained with passive modelocking techniques [15].

Passive modelocking in a laser system relies on the use of some kind of saturable absorber. The function of such a absorber may be summarized as that the optical loss of the device is smaller for higher intensities than for lower intensities. That can be real saturable absorbers like semiconductor saturable absorber mirrors (SESAM) or so called artificial saturable absorbers. Such artificial saturable absorber often rely on some nonlinear effect other than saturable absorption: Kerr-lens modelocking and nonlinear polarization evolution (NPE), which is also often called nonlinear polarization rotation (NPR). It is NPE that is a common modelocking mechanism used in fiber lasers. For such systems the nonlinear polarization rotation in a fiber together with some polarization optics forms a suitable passive modelocker that can be implemented using all-fiber components.

The compensation of group velocity dispersion in an all-fiber configuration is a more complex task as dispersion compensation usually relies on prisms pairs [7], diffraction gratings [8] or chirped mirrors [9]. The use of such bulk optical components detracts from the practical benefits of fiber. Photonic-Crystal fiber (PCF) and hollow-core photonic-bandgap fiber have been used for dispersion control in $1\mu m$ fiber lasers, but only with significant performance sacrifices [1].

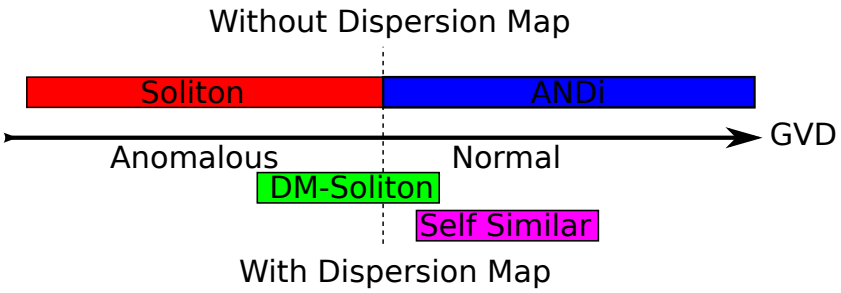

Figure 17: Different operating regimes according to their net total GVD

In general, a femtosecond laser consists of segments or components with both normal and anomalous GVD, where the net GVD can be normal or anomalous. Dependent on the net total GVD different mechanism form and shape the pulse and different classes of lasers can be distinguished (Figure 17).

Fiber lasers constructed entirely of fiber with anomalous GVD ($\lambda > 1.3\mu m$ in standard silica fiber) operate in the soliton regime and pulse energy is restricted by the soliton area theorem to $\sim 0.1nJ$. When incorporating small segments of normal GVD fiber such that the net GVD is still anomalous, soliton-like pulse shaping occurs as the nonlinearity balances the GVD. As the net GVD approaches zero, stretched pulse operation is observed [16]. A stretched-pulse laser has breathing solutions (dispersion-managed solitons), and in fiber lasers the pulse energy can be an order of magnitude higher than in a soliton fiber laser [17].

Cavities with large net normal dispersion were found to operate in the self-similar regime [18]. In the self-similar scheme a parabolic shaped pulse evolves self-similar, e.g. the pulse shape at any point in the cavity is a scaled version of any other point. In contrast to solitons or dispersion-managed solitons, self-similar pulses can tolerate strong nonlinearities without wave-breaking [1] resulting in higher output energies. Self-similar pulses are asymptotic solutions to the wave equation and the pulse duration evolves monotonic [18]. Such evolution cannot be a stable solution and some mechanism must be provided to reverse any changes and thus restore the solution after traversal of one roundtrip in the cavity. As due to the nonlinear phase accumulated in combination with

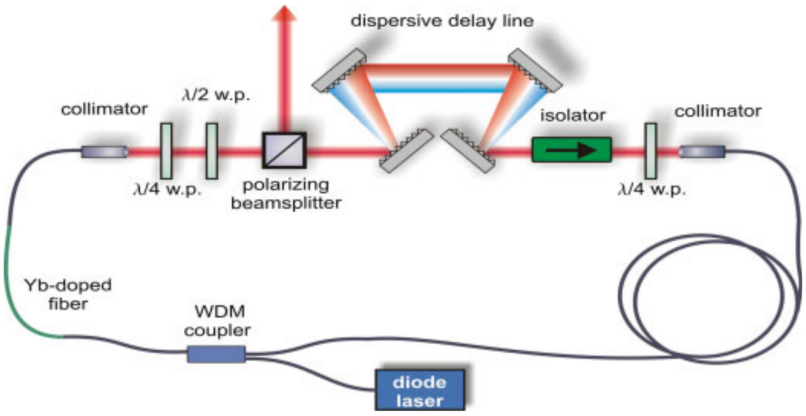

Figure 18: Scheme for self-similar laser [1]

normal GVD the pulses acquire positive linear chirp [1]. A schematic setup for such a laser can be seen in Figure 18. A dispersive delay line is used to dechirp the pulse after one round trip. The pulse is extracted from the cavity where it is expected to have maximum positive chirp and dechirped with diffraction gratings external to the cavity close to the transform limit, which implies an approximately linear chirp [1].

To design monolithic integrated fiber lasers it would be highly desirable to remove all components and parts providing anomalous dispersion and building an all-normal dispersion modelocked fiber laser.

4.2. Operation at Normal Dispersion

The first fiber laser reported working at all-normal dispersion was reported by Chong et al. in 2006. Pulse shaping is based on spectral filtering of a highly chirped pulse in the cavity. The setup can be seen in Figure 19.

When comparing the setup of Figure 19 with the self-similar setup of Figure 18 one can see that the setup is quite identical. Only the dispersive delay line was exchanged by a spectral filter.

The key elements of such a laser are a fairly long segment of single mode fiber, a short segment of gain fiber, a segment of SMF after the gain fiber, and components that

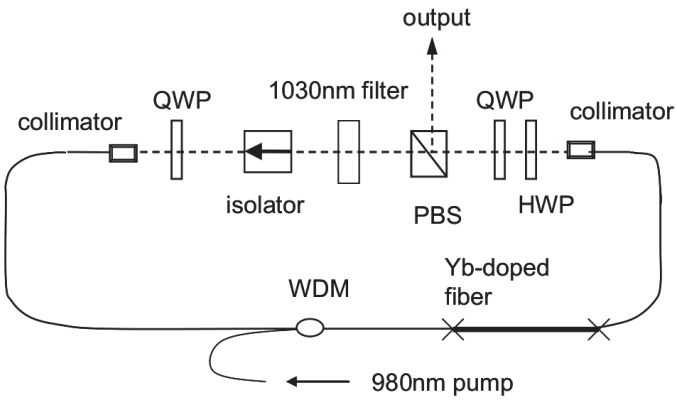

Figure 19: All normal dispersion fiber laser as of [10]

produce self-amplitude modulation [10]. It is the short segment of SMF after the gain fiber that impresses nonlinear phase shift on the pulse due to self phase modulation. Modelocking is implemented by NPE using the quarter wave plate (QWP) after the isolator to launch elliptically polarized light into the fiber and a half wave plate (HWP) and another quarter wave plate together with a polarizing beam splitter (PBS). The output is taken directly from the NPE ejection port.

Figure 20 depicts the properties of the cavity by showing typical simulated power spectra at different positions. After passing the spectral filter the power spectrum shows steep edges and a shape following the transmission curve of the filter (in this case a gaussian shaped top). In the first segment of SMF and the gain fiber the spectrum undergoes gentle spectral broadening. In the SMF segment after the gain fiber, with the amplified pulse, the enhanced peak power causes a substantial nonlinear phase shift. It is that phase shift that produces the characteristic sharp peaks at the edge of the spectrum. The saturable absorber (combination of QWP, HWP and PBS) reduces the peaks only slightly and it is the spectral filter which returns the power spectrum to its initial shape.

Self-amplitude modulation occurs in the saturable absorber and the spectral filter, but the effect of the spectral filter dominates. Therefore, the main pulse-shaping mechanism

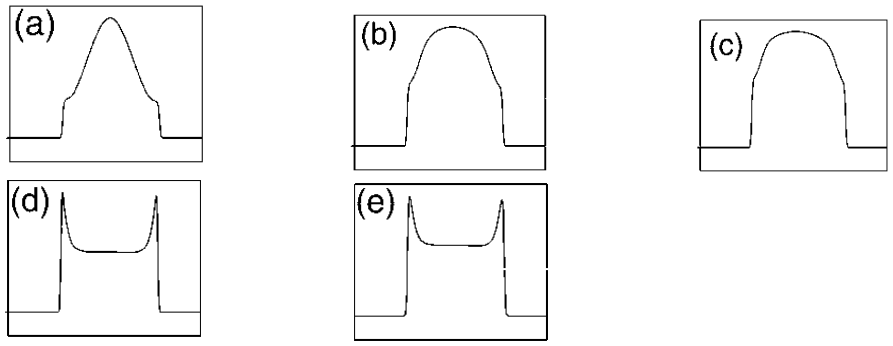

Figure 20: Spectrum at different positions inside the cavity (from [17]): (a) after the spectral Filter / Isolator, (b) at the beginning of the gain fiber, (c) after the gain fiber, (d) after the collimator following the gain fiber, (e) after the PBS. [Abscissa: Wavelength (a.u.), Ordinate: Intensity (a.u.). The scaling differs from plot to plot]

of an ANDi fiber laser can be described as chirped-pulse spectral filtering [17]. It is NPE that initiates the formation of pulses and the spectral filter that stabilizes modelocking.

4.3. Toward Monolithic Integration

As can be seen in the setup in Figure 19 a relative large amount of parts is made of free space optics between two collimators. As quarter-wave-plates and half-wave-plates can be replaced by fiber polarization controllers and polarization-beam-splitter also exist in fiber optics, Figure 21 shows a setup with nearly all fiber components. The only component not being integrated is the interference filter. This allows that the center wavelength of the oscillator can be tuned by tilting the filter. Previous setups with fiber integrated filters were reportedly not successful. To further integrate the setup and offering easy tunability and adjustment of the oscillator it was considered to replace the manual fiber polarization controller (FPC) with electric adjustable all-fiber polarization controllers. This allows to adjust the oscillator to either different operation parameters or to compensate environmental influences to some degree from a remote place. First the setup shown in Figure 21 was build using manual polarization controllers,

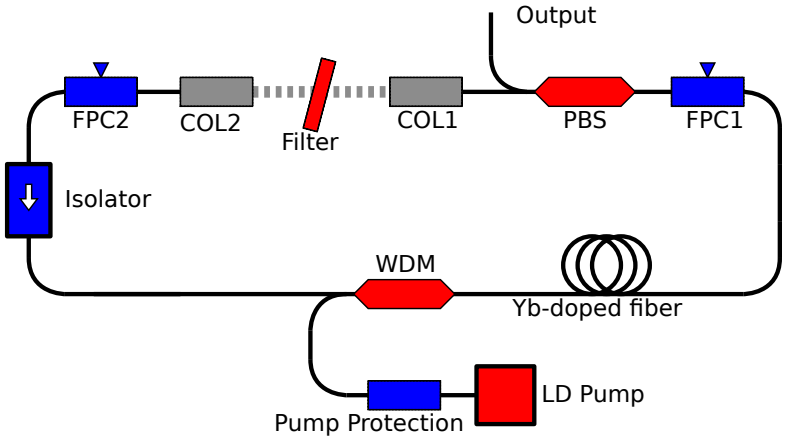

Figure 21: Modified ANDi Setup with Fiber Output

like General Photonic's PolaRITE^{TM}controllers or equivalent, to verify the oscillator is able to modelock and then to exchange one of the controllers with an automated one.

For choosing a suitable polarization controller the following points were considered:

1. All-Fiber Component
2. Operation Wavelength in the range from 1020nm to 1070nm
3. small size
4. simple electrical interface: no high voltages, high currents or frequencies
5. moderate price, comparable with manual ones, for controller and interface electronics

With that requirements some techniques like using piezoelectric actuators, electro-optic materials or stepper motor rotated wave-plates could be eliminated from the list. The polarization controller chosen was an All-Fiber Polarization Scanner-Controller from Phoenix Photonics. The controller was customized to use HI1060 fiber and characterized for operation in the preferred wavelength range. The controller consists of three segments, representing three all-fiber variable wave-plates, resulting in full coverage of the Poincaré sphere. This allows to translate any input state of polarization to any

required output polarization state. More details on the polarization controller and the electric interface will be given in the section dedicated to the Phoenix polarization controller.

4.4. Realization and Optimization of an ANDi Oscillator

The starting point for this work was an existing ANDi oscillator as shown in Figure 21 with an additional isolator at the output fiber. Degradation of the components had made modelocked operation impossible. Thus one-by-one the components were replaced by new components. First the isolator in the cavity was replaced. Since the actual pump power was not measured as a function of current through the diode, here for comparison the pump current is given instead of the pump power. At low pump power (320mA pump current), to avoid unintended modelock operation, the output power increased from 20mW to 30mW after replacing the isolator. Low fidelity ML operation could be achieved at maximum pump power (900mA pump current).

Next the PBS was replaced and the output power increased to around 36 mW but modelocking was not possible even at highest pump powers. As unabsorbed pump power could be measured at the output port, the length of active fiber was increased from 50cm to about 70cm. To lower the repetition rate an additional segment of SMF was spliced into the cavity. In this configuration the output power at 320mA reference pump current increased to 46mW and ML operation could be achieved at 750mA pump current producing 2.5nJ pulses at a repetition rate of 40.51 MHz as shown in Figure 22 and 23. As one can see the spectrum exhibits a large peak near the center that corresponds to the center wavelength of the continuous wave (CW) operation.

The oscillator was very sensitive to environmental influences, so a protective cover was build. After readjusting the free space section and tuning the filter center wavelength, self starting modelocking operation at 700mA was observed and was stable with pump current down to 600mA. Figure 24 shows the ouptut spectrum for different pump currents.

As the oscillator worked stable the electric polarization controller (EPC) was spliced

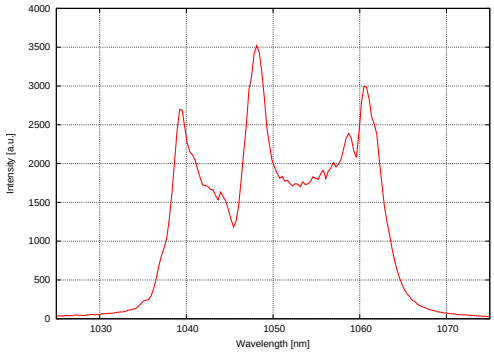

Figure 22: Output Spectrum of ANDi laser with $I = 750\text{mA}$

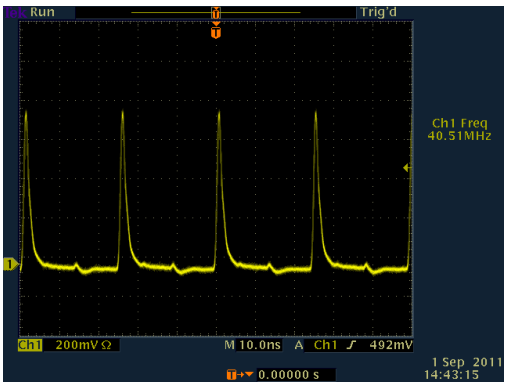

Figure 23: Output pulse train of ANDi laser with $I = 750\text{mA}$

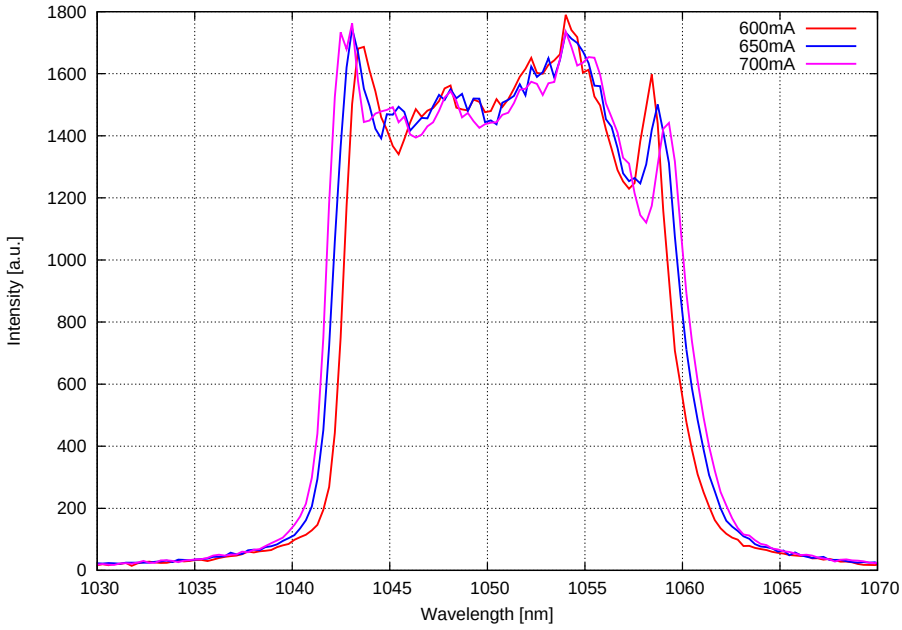

Figure 24: Output spectrum at different pump currents

into the cavity. The position of the EPC was chosen right after FPC2, as FPC1 purpose is not only to implement NPE but also to set the output coupling ratio together with the PBS. To verify the function of the EPC variation of only one parameter is desirable.

With the EPC in place the cavity could be modelocked and by adjusting the EPC via a computer interface, changes of FPC1 and FPC2 could be compensated. The resulting spectrum and pulse train taken with a photodiode and a sampling oscilloscope can be seen in Figure 25 and 26. The output energy was 2.67nJ at a repetition rate of 41.33 MHz.

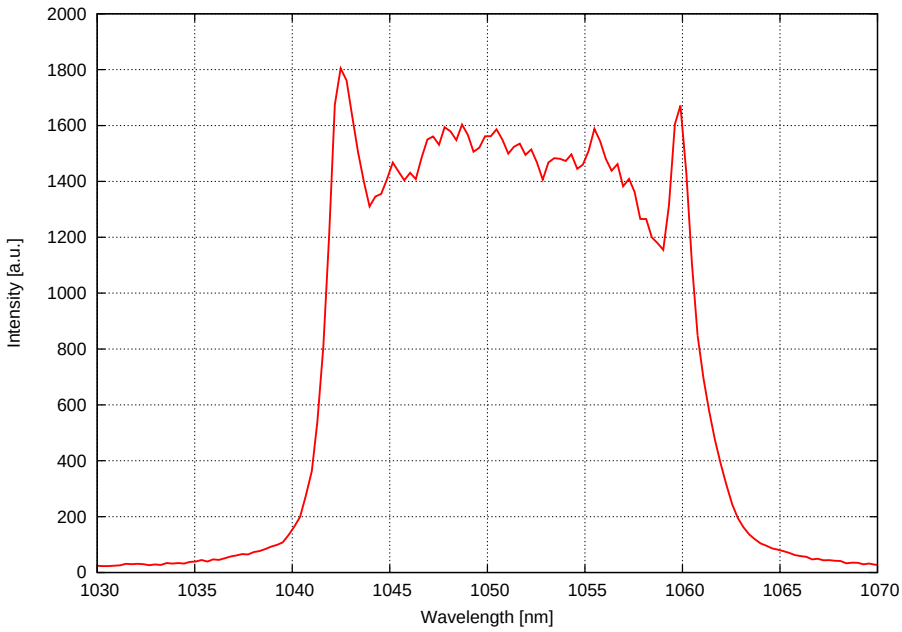

Figure 25: Output spectrum with EPC active, I=750mA

As FPC2 was removed completely it was not possible to obtain modelocking. This may result from the amount of SMF between FPC2 and the EPC, that was not shortened more to have enough fiber at the EPC to reuse it and splice it again. With FPC2 removed, the point where an elliptical polarization is set in the fiber and therefore the

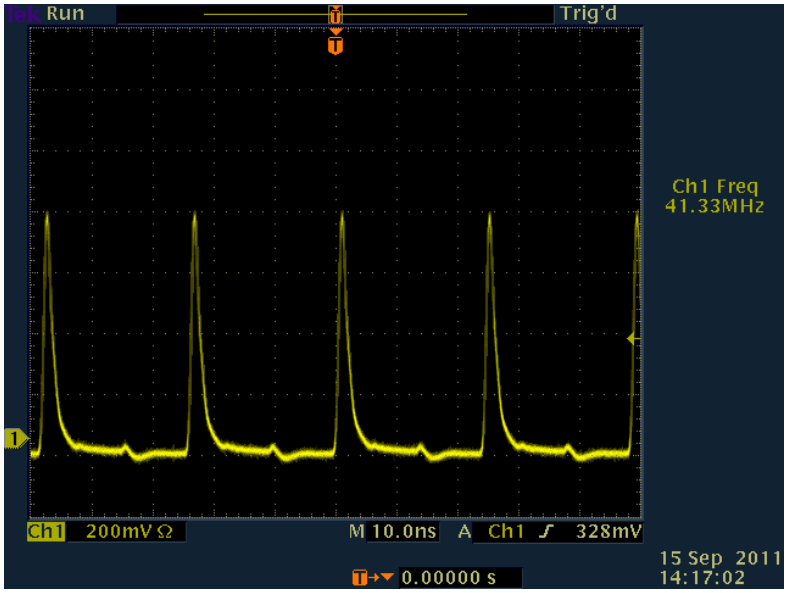

Figure 26: Output pulse train of ANDi laser with $I = 750\text{mA}$

length on which NPE acts is shorter by about 0.5m.

After spooling most of the fiber onto fiber spools and mounting the last fiber components to the breadboard the oscillator self-started modelocking at about 500mA pump current and could hold modelocking stable down to 450mA. At this point FPC2 could be removed completely while still being able to modelock the cavity.

The final cavity consists of the components listed in Table 1.

Manufacturer	**Part Number**	**Description**
AFW	ISOS-50	Polarization Insensitive Isolator at 1050nm
Opto-Link Corp.	OLCS-12-105	1x2 Port Polarization Beam Splitter at 1050nm
Thorlabs	FB1050-10	Bandpass Filter, CWL: 1050nm, FWHM: 10nm
Bookham	LC96AA74-20R	974nm, 600 mW kink free power
AFW	WDM-SM-9830-B-1-0	WDM 980nm / 1030nm, 1m bare fiber
OZ Optics	FPC-100	All-Fiber Polarization Controller
General Photonics	PLC-003	PolaRITE^{TM}, drop-in, Polarization Controller
Phoenix Photonics	PSC-10-0-0	All-Fiber Polarization Scanner-Controller
Corning	HI1060	HI1060 SMF
CorActive	Yb 164	SM, Yb doped, single clad, >400dB/m @ 976nm
Thorlabs	CFS5-1064-FC	Pigtailed Aspheric Collimators, 1064 nm

Table 1: Component List of ANDi laser

4.5. Results

To characterize the output pulses, the pulses were characterized using second harmonic frequency resolved optical gating. For this the rather long output pulses were compressed using a pair of gratings. The grating compressor was readjusted every time before measuring traces at different output couplings or pump currents.

Figure 27 shows the measured and reconstructed FROG trace for 1nJ output pulse energy, while Figure 28 shows the retrieved pulse and spectrum. The plots also include the measured output spectrum using an Ocean Optics spectrometer.

By increasing the pump current the output energy increased to 1.4nJ. Figure 29 and 30 show the resulting traces.

In the retrieved traces one can see that the pulses already broke up due to the high nonlinearities. Therefore a segment of SMF and the isolator at the fiber output were removed. After removing the extra isolator at the fiber output together with about 1m of SMF and angle cleaving the output another set of FROG traces were measured. These showed lower nonlinearities and pulse duration of about 160 fs.

Figure 31 shows the measured and reconstructed FROG trace for 1.8nJ output pulse energy after removing the isolator, while Figure 32 shows the retrieved pulse and spectrum.

By adjusting the output coupling ratio the pulse energy increased to 2.0nJ. The result can be seen in Figure 33 and 34.

The traces still show a considerable amount of higher order nonlinearities that are not compensated by the gratings compressor. By eliminating the losses in the output isolator and shortening the output fiber length the pulse energy doubled while showing slightly lower nonlinearities.

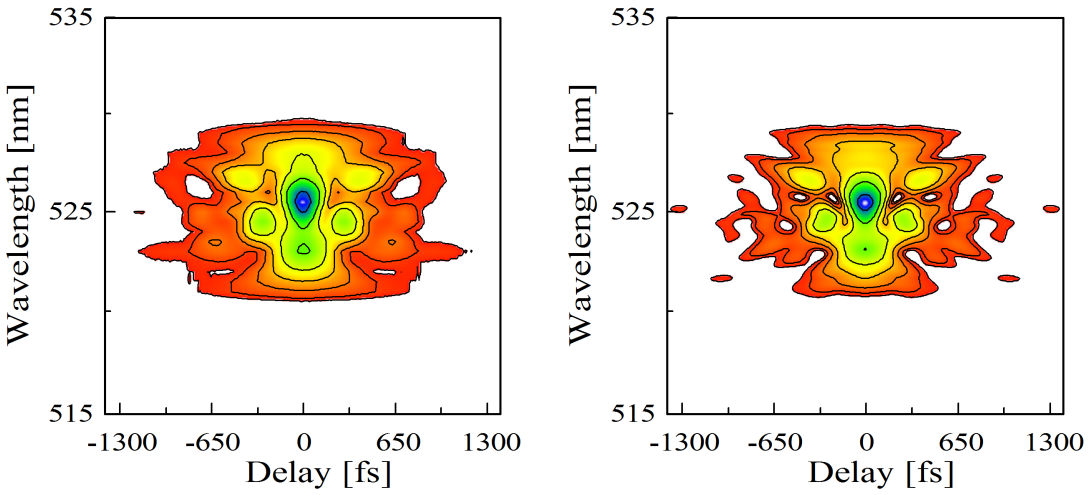

Figure 27: Measured (left) and reconstructed (right) FROG trace for 1nJ pulse energy

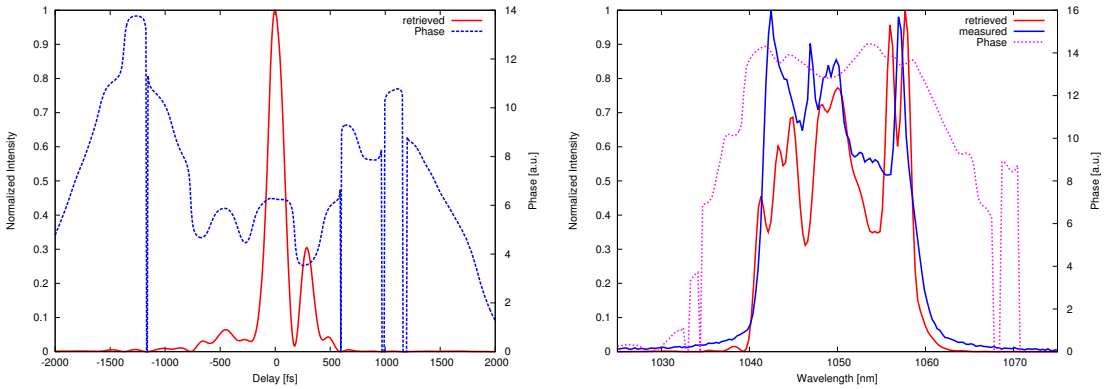

Figure 28: Retrieved pulse and spectrum for the 1nJ FROG in Figure 27

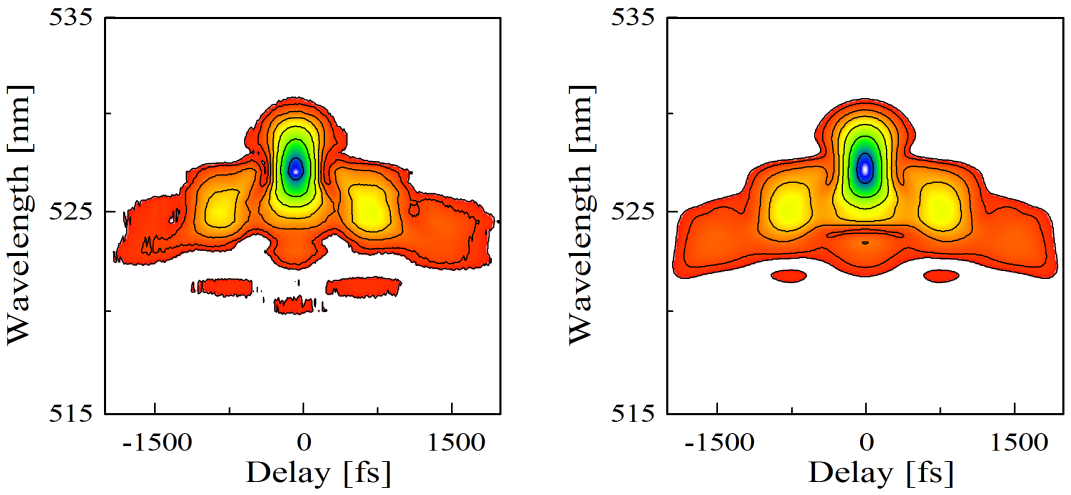

Figure 29: Measured (left) and reconstructed (right) FROG trace for 1.4nJ pulse energy

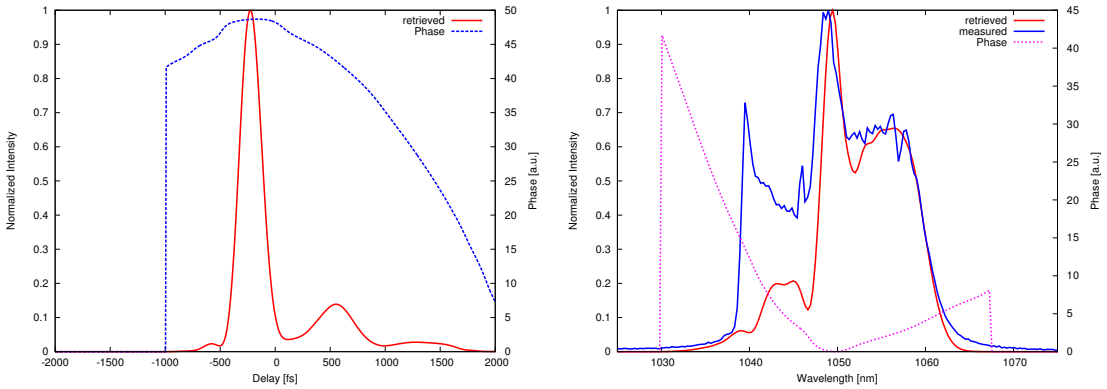

Figure 30: Retrieved pulse and spectrum for the 1.4nJ FROG in Figure 29

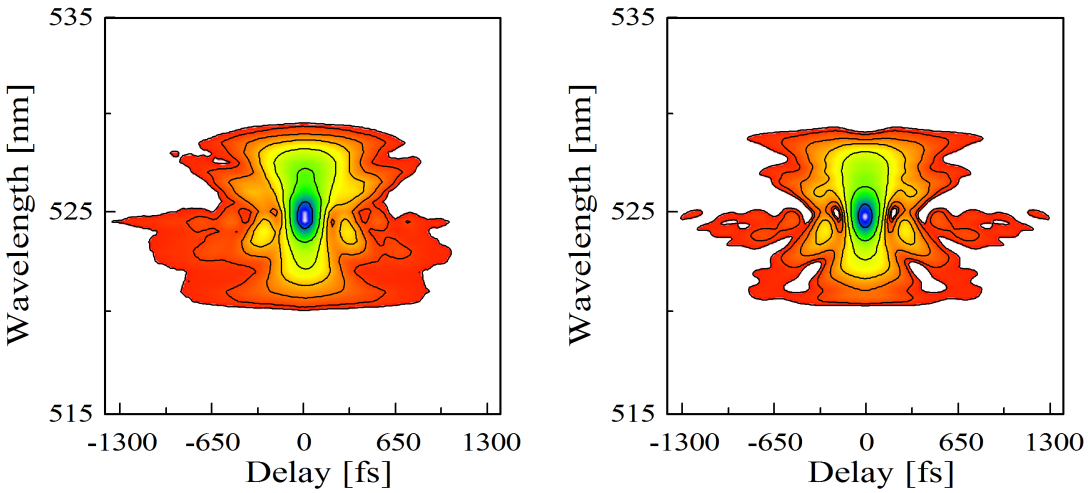

Figure 31: Measured (left) and reconstructed (right) FROG trace for 1.8nJ pulse energy, output isolator removed

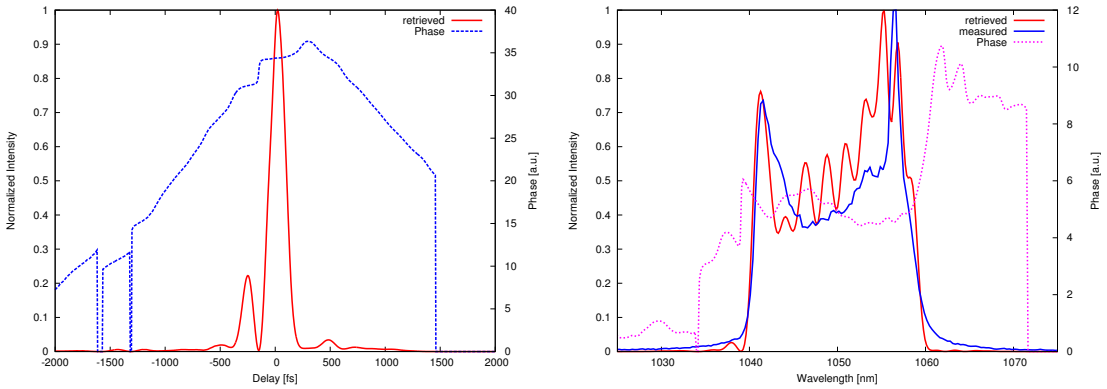

Figure 32: Retrieved pulse and spectrum for the 1.8nJ FROGin Figure 31
FWHM: 165.4 fs

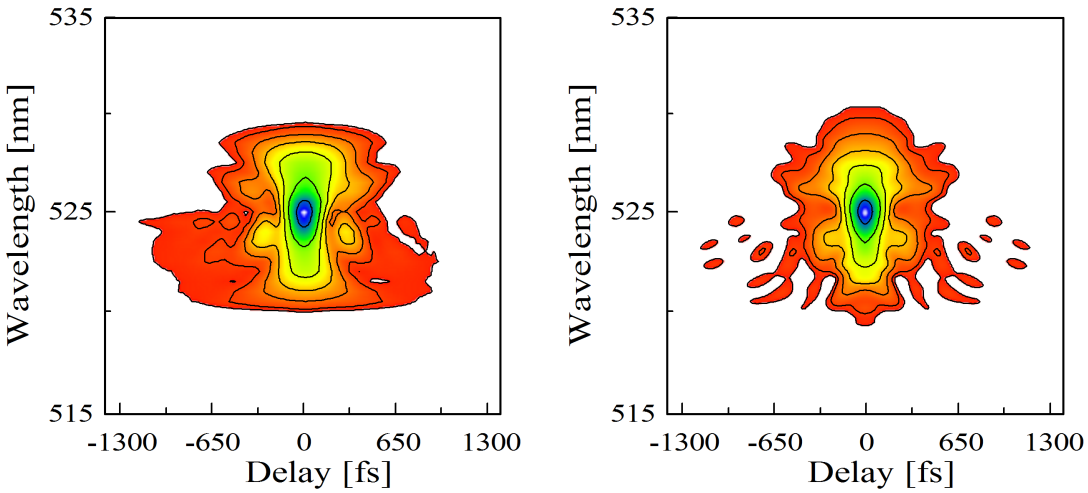

Figure 33: Measured (left) and reconstructed (right) FROG trace for 2.0nJ pulse energy, output isolator removed

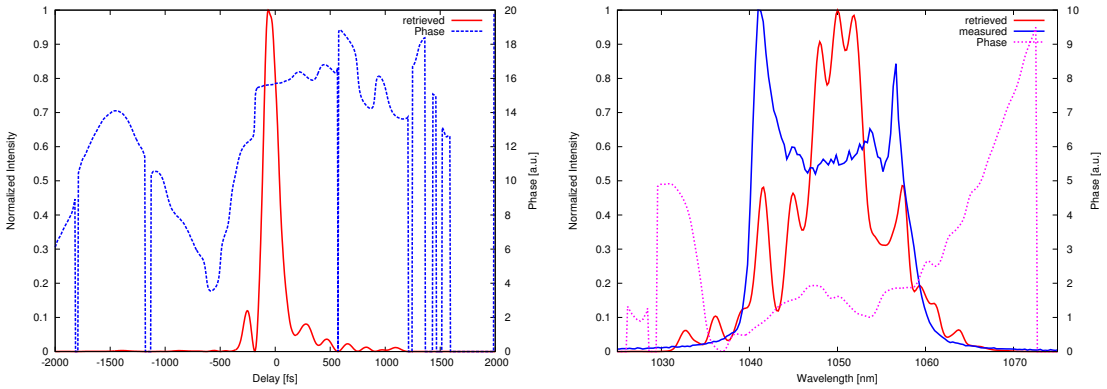

Figure 34: Retrieved pulse and spectrum for the 2.0nJ FROG in Figure 33
FWHM: 155.55 fs

5. Monolithic Fiber Chirped Pulse Amplification

5.1. Introduction

Chirped pulse amplification (CPA) is a method of amplifying ultrashort pulses by stretching them temporal prior to amplification and to compress them afterwards [19]. This technique was first introduced for radar systems and later adapted for optical amplification. This allows higher average output powers without altering the pulse properties due to nonlinearities and dispersion. Typical systems that are able to bring the nJ or sub-nJ output power of a fiber oscillator into the μJ range consist of multiple stages of amplifiers, to ensure good pulse quality. To prevent running into troubles with polarization such systems are preferably build using polarization maintaining fiber.

Ytterbium doped fiber amplifier (YDFA) have shown to be attractive scalable sources for seeding and pumping of carrier envelope-phase (CEP) stable difference frequency generation (DFG) optical parametric amplifiers (OPAs) [20].

YDFA amplifiers are also attractive due to their large bandwidth as compared to their crystalline counterparts [21] and build in fiber technology such system promise compact, robust, reliable turn-key operation.

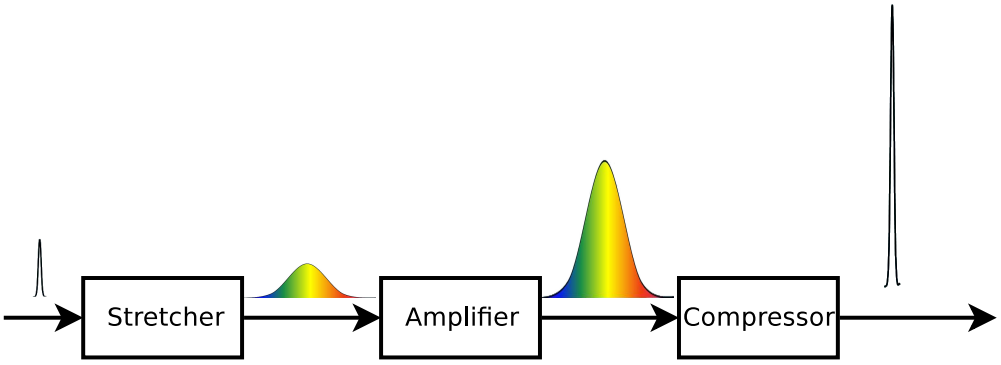

Figure 35: Schematic CPA System with pulse evolution shown

Figure 35 shows a simple one stage setup for a CPA system. It's main components are the stretcher at the input, an amplifier and the compressor at the output.

Ultrashort pulses from an oscillator are stretched temporally using a stretcher. Effi-

cient stretchers for fiber systems around $1\mu m$ wavelength can be build by using standard SMF (or PM fiber) utilizing normal dispersion. With sufficient long fiber pulses can be stretched from the fs into the ps range.

The amplifier may be build from Yb doped PM fiber pumped by a single or for high power amplifiers by multiple laser diode modules.

The compressor at the end reverses the chirp introduced by the stretcher and, if the amplification did not introduce much nonlinearities or higher-order dispersion, compresses the pulse back to the fs regime.

Another obvious technique for avoiding nonlinearities at amplification is instead of temporal scaling the pulse by spatial scaling: scaling the fiber core size. To reach highest powers both techniques of temporal and spatial scaling may be combined.

Fiber core size scaling beyond the single-mode limit while still maintaining diffraction-limited output rely on the fact that in a highly doped optical fiber amplifier pulse propagation length can be made significant shorter than the characteristic distance for power coupling from fundamental to higher-order modes [22].

According to equation 2.14 ($V = 2\pi/\lambda aNA = 2\pi/\lambda an_1\sqrt{2\Delta}$) by lowering the refractive index difference Δ between core and cladding the fiber core radius a can be increased. This results in lower acceptance angle, thus making it harder to couple light efficiently into the fiber, and increased bending losses [22]. An alternative is to increase the fiber core dimension without reducing the refractive index difference while leaving the single-mode regime. When using multi mode fibers one needs to take special precautions when coupling into the fiber and when coupling out. The mode field diameter (MFD) needs to be adjusted and by using a fiber taper single-mode excitation can be achieved. Thus in an ideal fiber the fundamental mode would propagate without being scattered into higher order modes. In a real fiber however, imperfections of the core can provide coupling between the fundamental mode and higher order modes and therefore destroying the beam quality and pulse shape. The ultrashort pulse shape get destroyed when propagating within different modes because every mode travels at a different group velocity.

5.2. An Amplifier

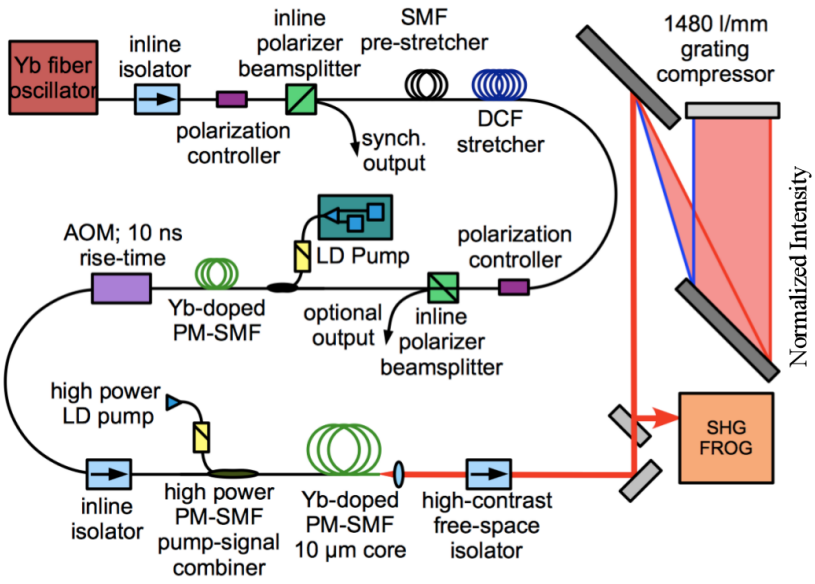

Figure 36: Setup of the monolithic ytterbium fiber amplifier

Figure 36 shows a setup for a monolithic ytterbium fiber amplifier. Stretching of the pulse is achieved by using a hybrid fiber stretcher consisting of ∼8m SMF followed by 100m of dispersion compensating fiber (DCF, from OFS) [23], stretching the pulses to ∼350ps. The stretched pulses are then preamplifier in a PM SMF preamplifier before being fed to a PM double-clad 10 μm core SMF power amplifier. Between the two stages a fiber pigtailed acousto-optic modulator (AOM) was inserted to reduce the repetition rate and to suppress amplified spontaneous emission (ASE). The isolator at the input of the amplifier system prevents reflection back to the seed oscillator. With the polarization controller and fiber polarization beam splitter following the isolator the input seed energy can be adjusted and a monitoring port for the timing of the AOM is available. The amplified pulses are dechirped (compressed) using a 1480 lines/mm grating compressor and were characterized using second harmonic generation (SHG) frequency resolved optical gating (FROG).

As the effective mode area of the DCF is rather small the pulses were pre-stretched

and the seed energy was limited to ∼0.3 nJ. This ensures that nonlinearities within the stretcher unit are kept low and so no spectral broadening was observed at the stretcher output. As the stretcher is build using non PM fiber, a polarization controller together with a polarization beam splitter with PM fiber outputs was included to ensure linear polarized output and to avoid polarization mode dispersion.

The pre-amplifier stage is build from 1.5m polarization maintaining highly doped ytterbium single mode fiber (PM-YDF-HI from Nufern) pumped by a single fiber pigtailed laser diode with about 700mW max output power at 976nm.

The fiber pigtailed AOM between the two stages reduced the repetition rate to 200 kHz.

The power amplifier consists of ∼2m of Yb-doped SMF double clad fiber with 10μm core (PM-YDF-10/125 from Nufern) pumped using a seed-pump combiner (LC2010520HP from AOFR) and using a 10W fiber coupled laser diode.

5.3. Results

To characterize this amplification setup the output pulses were measured using SHG FROG at different output pulse energies. In Figure 37 the measured traces are shown for total output energies of about 20nJ, 1μJ, 1.7μJ and 2.5μJ. For each output energy the compressor was readjusted to obtain best compressible pulses. For low pulse energies of about 20nJ the FROG traces show that nearly no nonlinear phase has been accumulated (Figure 38). For output energies up to about 1μJ the retrieved spectral phase does not deviate much from the phase obtained as reference at 20nJ and are therefor of high quality. The deviation from the Fourier-limited pulse duration of 150fs is solely due to a mismatch of the high order dispersion between the stretcher and compressor. From Figure 38 it can be seen that for total output pulse energies up to $\sim$ 1μJ almost all energy is contained in the main part of the pulse.

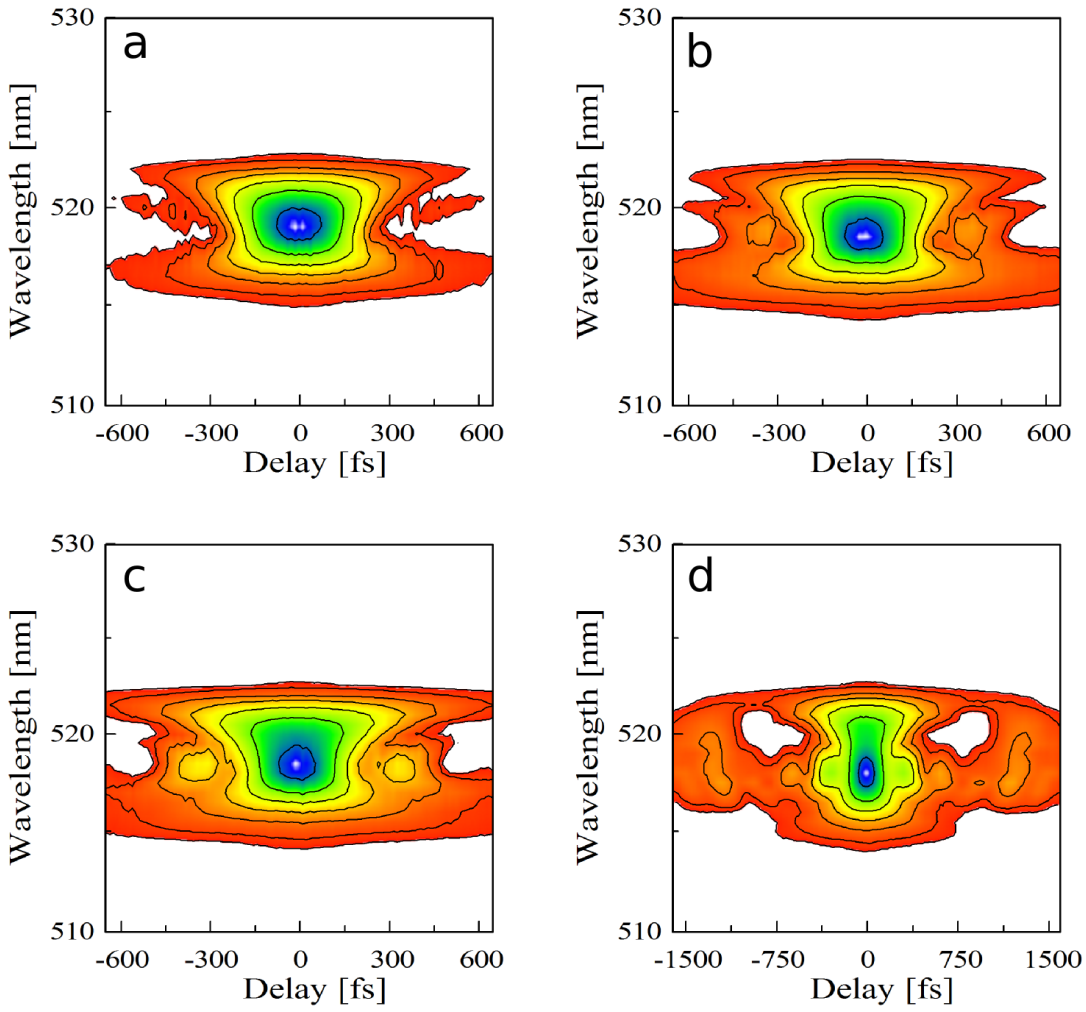

Figure 37: SHG FROG traces for output energies pf 20nJ (a), 1μJ (b), 1.7 μJ (c) and 2.5μJ (d). Please not a change in the scan range for 2.5μJ in subplot (d).

When increasing the output energy further to about 1.7μJ the pulse quality starts to decrease slightly, although the main part of the pulse can still be compressed to $\sim$ 200 fs and the pulse energy contained in the satellites and background is limited to less than 20 percent.

At about 2.5μJ the pulse satellites and background contain even more energy and already extend for more than 5 ps from the center of the pulse. Figure 37 shows that by a change in scan range and in Figure 38 the retrieved spectral phase change is clearly visible. For that pulse energy the peak power contained at the output is in the order of the peak power obtained for 1.7μJ due to the higher nonlinearities.

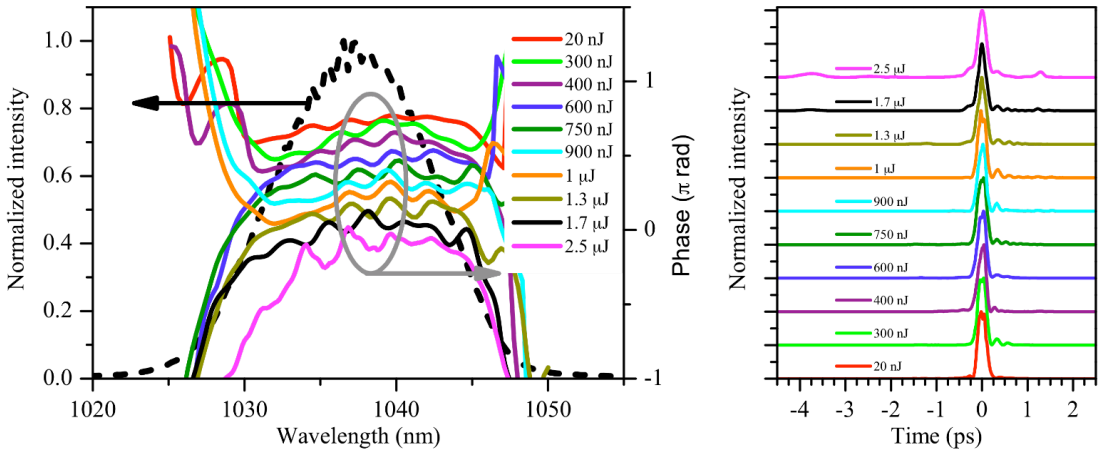

Figure 38: Retrieved spectral phase (left) and pulse envelope (right) at different output energies. For energies up to $\sim$1.7μJ the retrieved spectral phase does no differ much from the reference phase obtained at 20nJ. At 2.5μ a clear deviation of the spectral phase from the reference. In the right subplot for energies above 1μJ strong pulse distortion due to nonlinearities can be easily identified.

6. Polarization Controller Interface

6.1. Introduction

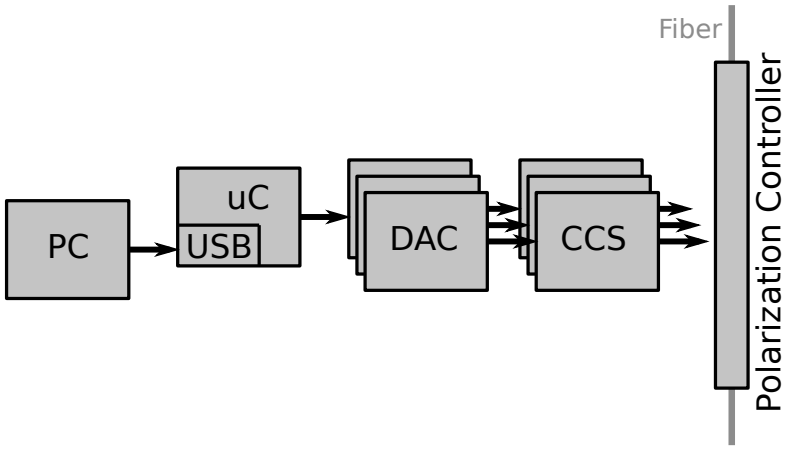

Figure 39: Polarization Controller Interface Electronics: A USB capable microcontroller (uC) interfaces a set of digital-to-analog converters (DAC) that control adjustable constant current sources (CCS).

The Phoenix Polarization controller offers three variable all-fiber waveplates to provide full coverage of the Poincaré sphere enabling conversion from any input state of polarization to any required output state. As the polarization controller is build in all-fiber technology it exhibits low insertion loss and high return loss.

The supplied information to the Phoenix Polarization Controller state a "simple current control" and the current that is needed for each segment to obtain a full cycle of polarization rotation. The specification state a current of about 36mA for 2π rotation at 1030nm. According to the datasheet the three all-fiber variable waveplates are characterized by only a resistance of about 139 Ω.

Due to that specifications it can be assumed that the polarization is not changed due to piezoelectric or electro-optical interaction. Also polarization manipulation due to other actuators like stepper motors can be excluded. As Phoenix Photonics has access to fiber side-polishing technology, it can be assumed that the device operates by manipulating

the polarization due to induced thermal stress through thermal losses in a resistive metal layers coated onto the fiber.

6.2. Electrical Interface

To interface the Phoenix Polarization Controller a computer interface electronic was developed. A simplified schematic can be seen in Figure 39.

The setup consist of multiple adjustable constant current sources that are controlled by a set of digital-to-analog converters (DAC). The voltage output digital-to-analog converters are interfaces by an 8-bit, USB capable, microcontroller. The microcontroller receives commands and data over the USB interface and sets the digital-to-analog converter according to it. The voltage set at the output of the digital-to-analog converter is then converted by an adjustable current source into a current that is fed through a segment of the polarization controller.

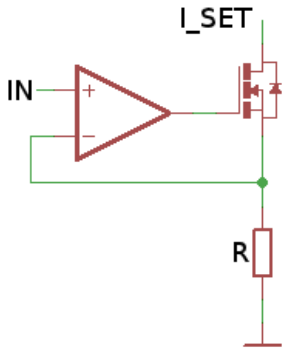

Figure 40: Basic current source

As the polarization rotation is somehow related to the current flowing through the controller segments a digital controlled current source was chosen as a basis. This basic current source in Figure 40 consists of a operational amplifier, a metal oxide field effect transistor (MOSFET) and a current sensing resistor (R). Its function can be summarized that a voltage applied on the terminal labeled IN (U_IN) is translated into a current proportional to I_SET = U_IN / R. In total nine constant current sources were implemented to allow to connect up to three polarization controllers with three segments each.

As digital-to-analog converter a 12bit type with 2.56V internal reference voltage was chosen. With a current sensing resistor of 39 Ω the current per bit can be calculated as follows:

$$\Delta I = \frac{2.56V}{4095}\frac{1}{39\Omega} \sim 16\mu A \tag{6.1}$$

So the degree of rotation for a single bit can be expressed, assuming linear relation and the current stated in datasheet for full rotation:

$$\Delta\phi = \frac{360°\Delta I}{I_{2\pi}} \sim 0.1° \tag{6.2}$$

with $I_{2\pi} \sim 55mA$

As computer side interface the universal serial bus (USB) was chosen in preference over the older serial interface RS232, because most modern computers or notebooks only support that interface. To ease programming on the computer side the device enumerates itself as a virtual serial interface using the USB communication device class (CDC) and therefore no special drivers are needed to be installed on most modern operating systems. To interact with the device a simple human readable protocol was implemented.

The complete schematics for the interface electronics is attached to the end of this section as Figure 43 and 44.

6.3. Communication Protocol

The protocol is kept very simple and only supports two commands: **set** and **get** for setting or getting the value of a current source. A get is followed by the channel to read the value from. The channels are named dac1 for the first channel up to dac9 for the ninth channel. So typing `get dac1` followed `enter` (carriage return or line feed) in a terminal will make the device respond: `dac1=x`, where `x` is the 12 bit value (0-4095) with which the digital-to-analog converter was loaded.

The set command is structured quiet similar: `set dac2 x`, where x is the 12 bit wide value, will set the digital-to-analog converter.

6.4. Results

To test the polarization controller and the developed interface electronics the measurement setup shown in Figure 41 was build. Linearly polarized light at 1030nm was coupled into the fiber input of the polarization controller using a translation stage and lens L1. The output of the polarization controller was collimated using lens L2. The polarization beam splitter PBS served as an polarization analyzer. The optical power after the PBS was recorded using a Coherent Fieldmax Power Meter. The half wave plate at the input was used to set the linear input polarization such that maximum power was measured at the power meter when the polarization controller is not interfaced and therefore does not induce any polarization rotation.

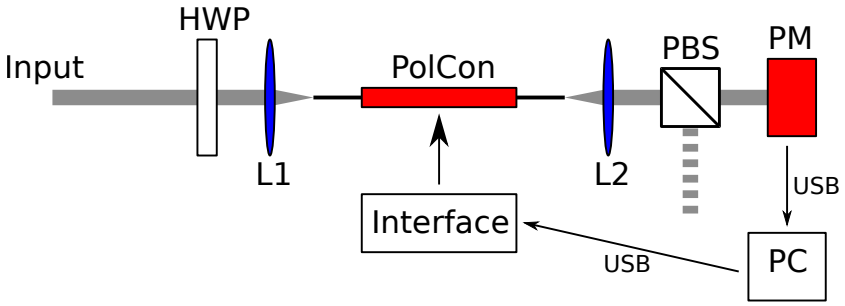

Figure 41: Test Setup for Polarization Controller. HWP: Half Wave Plate, L1 & L2 Lenses, PBS: Polarization Beam Splitter, PM: Power Meter

To automatize the step of recording the power vs. settings of the polarization controller a small computer based utility was developed using the USB interface of the power meter and the polarization controller interface electronics. The function of the utility can be summarized as follows: set a new polarization, wait for the power value to stabilize at the power meter, take some data points and average them, save power level and values set at the polarization controller.

A sample trace can be seen in Figure 42. The output power changes with the supplied DAC value almost like a sine curve. One can see that the maxima move closer together as the current increases. There is more than one period displayed as the polarization controller was designed for a full cycle of rotation at about 55mA from 1300nm to

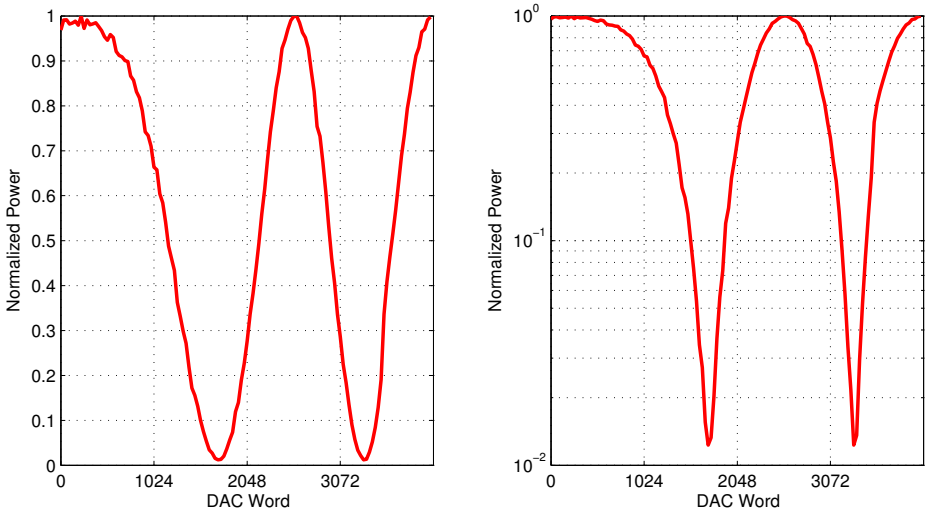

Figure 42: Measured Trace with Segment 1 sweeped over full range, other segments fixed. Left: linear plot, right: logarithmic plot

1610nm. For 1050nm a full rotation is obtained at only 35mA.

The calculated polarization polarization extinction ratio (PER) for the trace measured above was about 20 dB. With adding some additional rotation by setting the other segments current to some value the polarization extinction ratio could be increased to about 30dB.

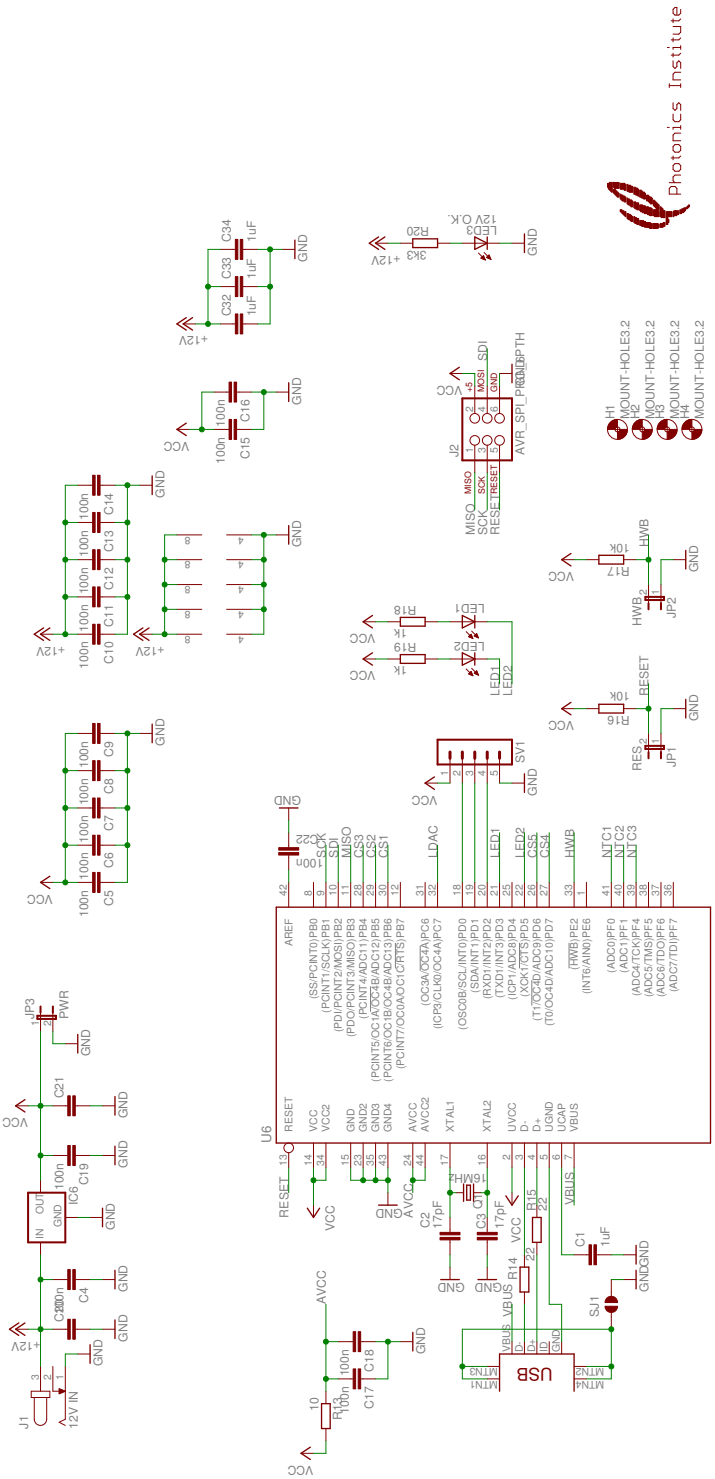

Figure 43: Schematics Polarization Controller Part 1

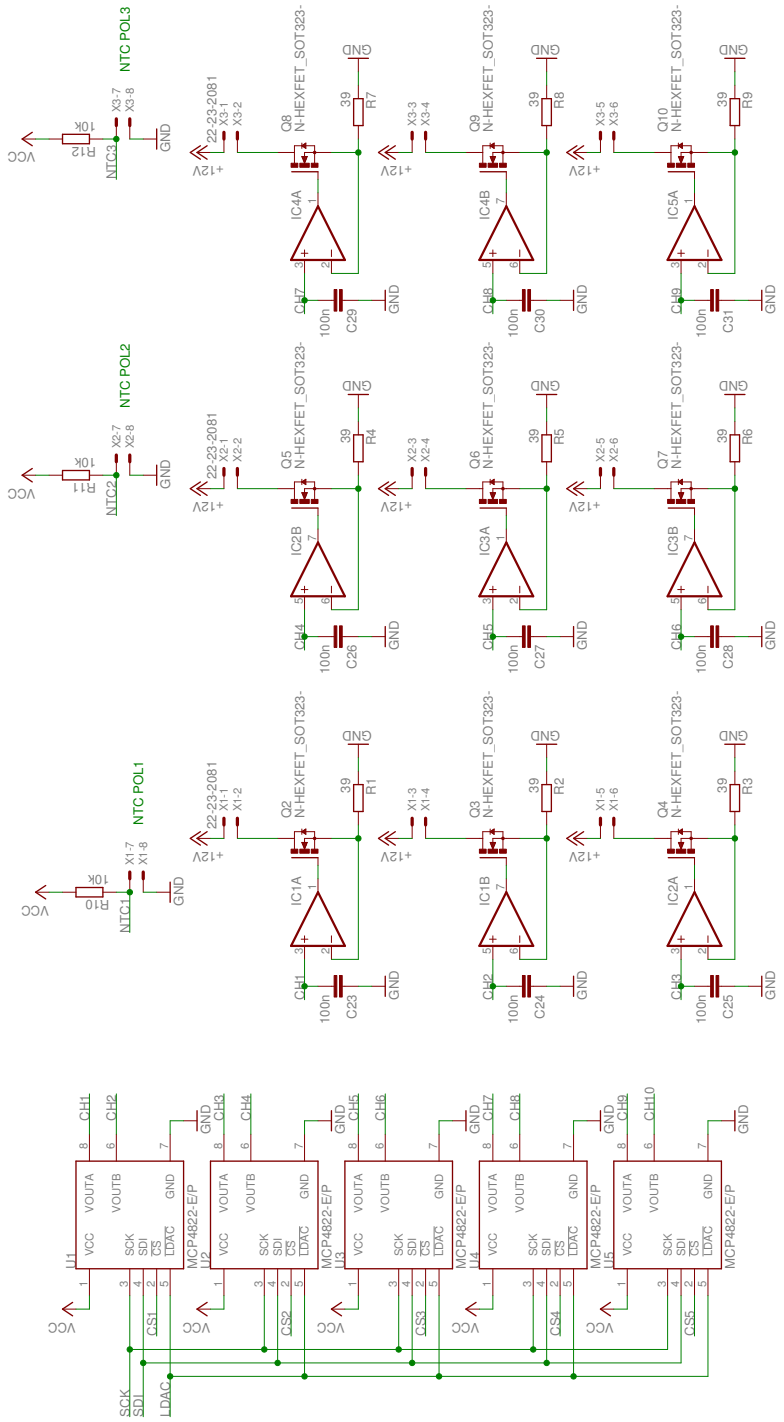

Figure 44: Schematics Polarization Controller Part 2

7. Conclusion and Outlook

This work demonstrated that electronic adjustable all-fiber polarization controllers can be used for polarization control in all-normal dispersion ytterbium fiber lasers allowing remote stabilization of the laser cavity and therefore bringing such systems closer to a reliable true turn key laser oscillator for industrial applications due to the low components count and the high level of fiber integration while allowing to tune the system.

With all-normal dispersion laser cavities incorporating electronic adjustable all-fiber polarization controllers the monolithic integration will lead to cheap, robust and reliable femtosecond light sources. The ability to tune output coupling and nonlinear polarization rotation from remote will allow a wide field of applications and unique stabilization techniques to a be applied. Recent works have shown the concept of all-normal dispersion fiber lasers with different rare earth ions like thulium[24] allowing to cover different wavelength ranges and therefore making such systems attractive for new applications like pump or seed sources for novel laser crystals.

A. List of Abbreviations

ANDi ..... All-Normal-Dispersion

AOM ..... Acousto-Optic Modulator

ASE ..... Amplified Spontaneous Emission

CDC ..... Communication Device Class

CEP ..... Carrier Envelope-Phase

CPA ..... Chirped Pulse Amplification

CW ..... Continous Wave

DAC ..... Digital-to-Analog Converter

DCF ..... Dispersion Compensating Fiber

DFG ..... Difference Frequency Generation

EDFA ..... Erbium Doped Fiber Amplifier

EPC ..... Electric Polarization Controller

FPC ..... Fiber Polarization Controller

FROG ..... Frequency-Resolved Optical Gating

GVD ..... Group Velocity Dispersion

HWP ..... Half Wave Plate

MFD ..... Mode Field Diameter

ML ..... Modelocking

MOSFET ..... Metal Oxide Field Effect Transistor

NA ..... Numerical Aperture

NPE ..... Nonlinear Polarization Evolution

NPR ..... Nonlinear Polarization Rotation

OPA ..... Optical Parametric Amplifier

PBS ..... Polarizing Beam Splitter

PCF ..... Photonic-Crystal Fiber

PER ..... Polarization Extinction Ratio

PM ..... Polarization Maintaining

QWP ..... Quarter Wave Plate

SESAM ..... Semiconductor Saturable Absorber Mirror

SHG ..... Second Harmonic Generation

SMF ..... Single Mode Fiber

SPM ..... Self Phase Modulation

SSFM ..... Split Step Fourier Method

TOD ..... Third Order Dispersion

USB ..... Universal Serial Bus

XPM ..... Cross Phase Modulation

YDFA ..... Ytterbium Doped Fiber Amplifier

B. List of Figures

C. References

[1] F.W. Wise, A. Chong, and W.H. Renninger. High-energy femtosecond fiber lasers based on pulse propagation at normal dispersion. *Laser & Photonics Reviews*, 2(1-2):58–73, 2008.

[2] E. Snitzer. Proposed Fiber Cavities for Optical Masers. *Journal of Applied Physics*, 32(1):36–39, 1961.

[3] E. Snitzer. Optical maser action of ND^{+3} in a barium crown glass. *Phys. Rev. Lett.*, 7:444–446, Dec 1961.

[4] S. Poole, D. Payne, R. Mears, M. Fermann, and R. Laming. Fabrication and characterization of low-loss optical fibers containing rare-earth ions. *Lightwave Technology, Journal of*, 4(7):870 – 876, jul 1986.

[5] D.C. Hanna, R.M. Percival, I.R. Perry, R.G. Smart, P.J.M. Suni, J.E. Townsend, and A.C. Tropper. Continuous-wave oscillation of a monomode ytterbium-doped fibre laser. In *All-Fibre Devices, IEE Colloquium on*, pages 14/1 –14/4, jun 1988.

[6] M I Dzhibladze, Z G Ésiashvili, É Sh Teplitskiĭ, S K Isaev, and V R Sagaradze. Mode locking in a fiber laser. *Soviet Journal of Quantum Electronics*, 13(2):245, 1983.

[7] R. L. Fork, O. E. Martinez, and J. P. Gordon. Negative dispersion using pairs of prisms. *Opt. Lett.*, 9(5):150–152, May 1984.

[8] E. Treacy. Optical pulse compression with diffraction gratings. *Quantum Electronics, IEEE Journal of*, 5(9):454 – 458, sep 1969.

[9] Robert Szipöcs, Kárpát Ferencz, Christian Spielmann, and Ferenc Krausz. Chirped multilayer coatings for broadband dispersion control in femtosecond lasers. *Opt. Lett.*, 19(3):201–203, Feb 1994.

[10] Andy Chong, Joel Buckley, Will Renninger, and Frank Wise. All-normal-dispersion femtosecond fiber laser. *Opt. Express*, 14(21):10095–10100, Oct 2006.

[11] Andy Chong, William H. Renninger, and Frank W. Wise. All-normal-dispersion femtosecond fiber laser with pulse energy above 20nj. *Opt. Lett.*, 32(16):2408–2410, Aug 2007.

[12] G. Agrawal. *Nonlinear Fiber Optics*. Academic Press, 3 edition, January 2001.

[13] John M. Senior. *Optical fiber communications : principles and practice / John M. Senior*. Prentice Hall, New York :, 2nd ed. edition, 1992.

[14] M. Hofer, M. E. Fermann, F. Haberl, M. H. Ober, and A. J. Schmidt. Mode locking with cross-phase and self-phase modulation. *Opt. Lett.*, 16(7):502–504, Apr 1991.

[15] M.E. Fermann and I. Hartl. Ultrafast fiber laser technology. *Selected Topics in Quantum Electronics, IEEE Journal of*, 15(1):191 –206, jan. 2009.

[16] K. Tamura, E. P. Ippen, H. A. Haus, and L. E. Nelson. 77-fs pulse generation from a stretched-pulse mode-locked all-fiber ring laser. *Opt. Lett.*, 18(13):1080–1082, Jul 1993.

[17] Andy Chong, William H. Renninger, and Frank W. Wise. Properties of normal-dispersion femtosecond fiber lasers. *J. Opt. Soc. Am. B*, 25(2):140–148, Feb 2008.

[18] Fatih Ö. Ilday, Joel R. Buckley, and Frank W. Wise. Self-similar evolution of parabolic pulses in a fiber laser. In *Nonlinear Guided Waves and Their Applications*, page MD8. Optical Society of America, 2004.

[19] Donna Strickland and Gerard Mourou. Compression of amplified chirped optical pulses. *Optics Communications*, 56(3):219 – 221, 1985.

[20] O. D. Mücke, D. Sidorov, P. Dombi, A. Pugžlys, A. Baltuška, S. Ališauskas, V. Smilgevičius, J. Pocius, L. Giniūnas, R. Danielius, and N. Forget. Scalable yb-mopa-driven carrier-envelope phase-stable few-cycle parametric amplifier at 1.5 μm. *Opt. Lett.*, 34(2):118–120, Jan 2009.

[21] A. Fernández, L. Zhu, A. Verhoef, D. Sidorov-Biryukov, A. Pugzlys, A. Galvanauskas, F. Ilday, and A. Baltuška. Pulse fidelity control in a 20-μ sub-200-fs monolithic yb-fiber amplifier. *Laser Physics*, 21:1329–1335, 2011. 10.1134/S1054660X11130111.

[22] Martin E. Fermann, Almantas Galvanauskas, and Gregg Sucha. *Ultrafast Lasers: Technology and Applications (Optical Engineering)*. CRC, 2003.

[23] Lars Grüner-Nielsen, Dan Jakobsen, Kim G. Jespersen, and Bera Pálsdóttir. A stretcher fiber for use in fs chirped pulse yb amplifiers. *Opt. Express*, 18(4):3768–3773, Feb 2010.

[24] H. Liu, K. Kieu, S. Lefrancois, W.H. Renninger, A. Chong, and F.W. Wise. Tm fiber laser mode-locked at large normal dispersion. In *Lasers and Electro-Optics (CLEO), 2011 Conference on*, pages 1 –2, may 2011.

Acknowledgments

I would like to thank all people that supported my studies and this master thesis. First of all I would like to thank Prof. Andrius Baltuška for giving me the opportunity to join and work in his research group. Next I would like to thank my supervisors Dr. Alma del Carmen Ferńandez González and Dr. Aart Jan Verhoef that opened the very interesting world of fiber laser technology to me and supported my work with their great knowledge and kept supporting me after the birth of their son Sijmon. I would also like to thank the other group members for their help and support, especially Dr. Lingxiao Zhu. Finally, I want to thank my family, my girlfriend Martina and all other friends. Without their support my studies wouldn't have been possible.